Weierstraß-Institut
für Angewandte Analysis und Stochastik
Leibniz-Institut im Forschungsverbund Berlin e. V.

Preprint ISSN 2198-5855

Assessment of reduced order Kalman filter for parameter identification in one-dimensional blood flow models using experimental data

Alfonso Caiazzo[1], Federica Caforio[2], Gino Montecinos[3],

Lucas O. Müller[4], Pablo J. Blanco[5], Eleutero F. Toro[6]

submitted: April 20, 2016

[1] Weierstrass Institute
Mohrenstr. 39
10117 Berlin, Germany
E-Mail: alfonso.caiazzo@wias-berlin.de

[2] University of Trento
Via Mesiano 77
38123 Trento, Italy
E-Mail: federica.caforio@inria.fr

[3] CMM Universidad de Chile
Beauchef 851
Santiago, Chile
E-Mail: gmontecinos@dim.uchile.cl

[4] Laboratório Nacional de Computação Científica
Av. Getúlio Vargas 333
Petrópolis - RJ, Brazil
E-Mail: lomueller@lncc.br

[5] Laboratório Nacional de Computação Científica
Av. Getúlio Vargas 333
Petrópolis - RJ, Brazil
E-Mail: pjblanco@lncc.br

[6] University of Trento
Via Mesiano 77
38123 Trento, Italy
E-Mail: toroe@ing.unitn.it

No. 2248
Berlin 2016

2010 *Physics and Astronomy Classification Scheme.* 07.05.Tp, 47.11.-j, 47.63.Cb.

Key words and phrases. Blood flow, one-dimensional model, Kalman filter, parameter estimation, finite volume method.

Edited by
Weierstraß-Institut für Angewandte Analysis und Stochastik (WIAS)
Leibniz-Institut im Forschungsverbund Berlin e. V.
Mohrenstraße 39
10117 Berlin
Germany

Fax: +49 30 20372-303
E-Mail: preprint@wias-berlin.de
World Wide Web: http://www.wias-berlin.de/

Abstract

This work presents a detailed investigation of a parameter estimation approach based on the reduced order unscented Kalman filter (ROUKF) in the context of one-dimensional blood flow models. In particular, the main aims of this study are (i) to investigate the effect of using real measurements vs. synthetic data (i.e., numerical results of the same in silico model, perturbed with white noise) for the estimation and (ii) to identify potential difficulties and limitations of the approach in clinically realistic applications in order to assess the applicability of the filter to such setups. For these purposes, our numerical study is based on the in vitro model of the arterial network described by [Alastruey et al. 2011, J. Biomech. **44**], for which experimental flow and pressure measurements are available at few selected locations. In order to mimic clinically relevant situations, we focus on the estimation of terminal resistances and arterial wall parameters related to vessel mechanics (Young's modulus and thickness) using few experimental observations (at most a single pressure or flow measurement per vessel). In all cases, we first perform a theoretical identifiability analysis based on the generalized sensitivity function, comparing then the results obtained with the ROUKF, using either synthetic or experimental data, to results obtained using reference parameters and to available measurements.

1 Introduction

One-dimensional blood flow models provide a powerful tool to simulate complex cardiovascular conditions. These models have been validated versus in vitro experiments [19, 1, 4, 14] and in vivo measurements [31, 34, 33, 28, 5] and have proved to provide useful insights for the understanding of cardiovascular physiology and pathology (see, e.g., [2, 17, 16, 13, 30, 6, 23]).

One way to enhance the predictive and descriptive capabilities of models regarding clinically relevant applications, is to tune model parameters in order to perform patient-specific simulations. In order to do so, geometrical and physical parameters need to be adjusted to capture the features of specific subjects. This is the focus of data assimilation and parameter estimation methods, i.e., algorithms that combine mathematical models with available measurements in order to improve the accuracy of model predictions according to available observations.

We focus on the Kalman filter, a sequential approach in which estimates for state and parameters are corrected at each time step of the simulation, taking into account the error between the available measurements and the current numerical predictions. In particular, the reduced-order unscented Kalman filter (ROUKF) [20] has the advantages of not requiring the solution of a tangent problem, as it is based on an efficient sampling of the parameter space (through the so-called *sigma points*). Recently, the ROUKF has been successfully employed in the field of blood flow simulations for the estimation of the mechanical properties of the aorta [3] and to tune lumped parameter (0D) models used as boundary condition for 3D models according to patient data [32].

However, to the best of our knowledge, the only previous work dealing with the ROUKF and

one-dimensional models is the one by Lombardi [18], in which only in silico data (e.g. numerical results obtained with the very same model that defines the direct problem, perturbed with Gaussian noise) were used to feed the filter, and the number of measurement points per observed vessel was as big as the vessel spatial discretization (one data for each computational cell). In this work, as a further step towards the assessment of ROUKF in clinically realistic settings, we consider the in vitro arterial network described in [19, 1], for which parameter values have been determined prior to the experiment, and, at the same time, experimental flow and pressure measurements are available at selected points over the network (at most one measurement location per vessel). The latter aspect is particularly relevant when aiming at the application of this methodology in clinical cases, where measurements are usually available at only a few locations. A remarkable example of the application of parameter estimation to one-dimensional blood flow models is the one presented in [8]. However, in that work the methodology employed relied on the ensemble Kalman filter, which is different from the ROUKF examined here.

Focusing on this experimental setting, our main goal is the investigation of the accuracy and of the robustness of the ROUKF. Specifically, we present two sets of numerical tests, considering the estimation of (i) terminal resistances used for imposing boundary conditions and (ii) arterial wall parameters (such as Young's modulus and vessel thickness). In both cases, we present a case considering several unknown parameters (16 resistances and 8 thicknesses), and a test focusing on few parameters (two resistances on the same terminal branch and a single Young's modulus). While the former setup aims at assessing the robustness of the estimator, the latter has the scope of investigating the accuracy of the final estimate. For all presented numerical studies, we compare the results using perturbed in silico measurements with those obtained using in vitro data from [1], assumed to be located at the middle point of each observed vessel. Furthermore, the filter performance and its identification capabilities using either flow or pressure measurements are studied. In order to solve the one-dimensional blood flow model, corresponding to the experimental network, we consider the finite volume numerical method described in [27, 21, 25].

The rest of the paper is organized as follows. In Section 2 we shortly introduce the numerical method for the solution of one dimensional blood flow models, the reduced unscented Kalman filter and the considered in vitro arterial model. The assessment of the estimation algorithm with in silico and in vitro measurements is then presented in Sections 3 (terminal resistances) and 4 (arterial wall parameters). Finally, Section 5 draws the conclusions and the perspectives for future studies.

2 Methods

2.1 One-dimensional blood flow model

One-dimensional models are a suitable approach to investigate wave propagation phenomena in large arterial and venous networks. In fact, they deliver useful information on pressure and flow waveforms, while keeping the computational cost reasonably low. The set of equations

under study is

$$\begin{cases} \dfrac{\partial A}{\partial t} + \dfrac{\partial q}{\partial x} = 0, \\ \dfrac{\partial q}{\partial t} + \dfrac{\partial}{\partial x}\left(\dfrac{q^2}{A}\right) + \dfrac{A}{\rho}\dfrac{\partial p}{\partial x} = f, \end{cases} \tag{1}$$

where $A(x,t)$ is the cross-sectional area, $q(x,t)$ is the mass flow rate, $p(x,t)$ the average blood pressure over the cross section, $f(x,t)$ stands for the friction force per unit length and ρ denotes the blood density. We close system (1) with a constitutive law (usually called *tube law*) that relates the strain and strain rate of the vessel to the internal pressure [11] via the following relation

$$p(x,t) = p_e(x,t) + K(x)\phi(A(x,t),A_0(x)) + \frac{\Gamma}{A_0(x)\sqrt{A(x,t)}}\frac{\partial A}{\partial t}, \tag{2}$$

with

$$\phi(A,A_0) = \left(\frac{A}{A_0}\right)^m - \left(\frac{A}{A_0}\right)^n + p_0, \tag{3}$$

where $p_e(x,t)$ denotes the external pressure, $K(x)$ is related to the geometrical and mechanical properties of the vessel wall, since it is a function of the Young's modulus, the wall thickness and $A_0(x)$, which is the cross-sectional area at a reference pressure p_0. In turn, Γ is related to the viscosity of the vessel wall [1].

It can be easily observed that the viscoelastic term of tube law (2) results in a diffusive term in the momentum balance equation. Moreover, the spatial variation of mechanical and geometrical properties might give rise to extra source terms in the momentum balance equation. These source terms involve the product of the spatial derivative of a parameter and one of the unknowns. Such terms are called geometric source terms and their discretization must be carefully performed if explicit numerical schemes are to be used. Here we adopt the model proposed in [21], which consists in a reformulation of (1) that yields a first-order hyperbolic system with stiff source terms. A key ingredient of this reformulation is the introduction of an auxiliary variable Ψ, a relaxation parameter ε and an evolution equation

$$\frac{\partial \Psi}{\partial t} = \frac{1}{\varepsilon}\left(\frac{\partial q}{\partial x} - \Psi\right), \tag{4}$$

such that

$$\Psi \to \frac{\partial q}{\partial x}, \quad \varepsilon \to 0. \tag{5}$$

Considering (4) and (5), and replacing

$$\frac{\partial A}{\partial t} = -\frac{\partial q}{\partial x} = -\Psi + O(\varepsilon),$$

in (2), system (1) reads

$$\partial_t \mathbf{Q} + \mathbf{A}(\mathbf{Q})\partial_x \mathbf{Q} = \mathbf{S}(\mathbf{Q}), \tag{6}$$

in terms of the unknowns

$$\mathbf{Q} = [A, q, K, A_0, p_e, \Psi]^T, \tag{7}$$

with source term vector

$$\mathbf{S}(\mathbf{Q}) = [0, -f, 0, 0, 0, -\tfrac{1}{\varepsilon}\Psi]^T \tag{8}$$

and the coefficient matrix $\mathbf{A}(\mathbf{Q})$ given by

$$\mathbf{A}(\mathbf{Q}) = \begin{bmatrix} 0 & 1 & 0 & 0 & 0 & 0 \\ c^2 - u^2 + \frac{a_\Gamma}{2} & 2u & \frac{A}{\rho}\phi & \frac{A}{A_0}\left(a_\Gamma - c^2\right) & \frac{A}{\rho} & -\frac{A}{\rho}\frac{\Gamma}{A_0\sqrt{A}} \\ 0 & 0 & 0 & 0 & 0 & 0 \\ 0 & 0 & 0 & 0 & 0 & 0 \\ 0 & 0 & 0 & 0 & 0 & 0 \\ 0 & -\frac{1}{\varepsilon} & 0 & 0 & 0 & 0 \end{bmatrix}, \tag{9}$$

where

$$c^2 = \frac{A}{\rho} K \frac{\partial \phi}{\partial A}\,, \quad u = \frac{q}{A}\,, \quad a_\Gamma = \frac{\frac{\Gamma}{A_0\sqrt{A}}\Psi}{\rho}\,. \tag{10}$$

Note that we are considering the trivial evolution equations

$$\frac{\partial K}{\partial t} = 0 \quad , \frac{\partial A_0}{\partial t} = 0 \quad , \frac{\partial p_e}{\partial t} = F(x,t)\,,$$

with $F(x,t)$ prescribed, as proposed by [37]. Doing so incorporates the variation of geometrical and mechanical properties in the eigen-structure of the system and allows for the development of well-balanced numerical schemes for one-dimensional blood flow models [27]. See [21] for details on the derivation of (6) and for a complete mathematical analysis of the system.

System (6) is numerically solved using the high-order ADER finite volume scheme [38], with the DET solver for the generalized Riemann problem (GRP) [9]. As it is well known, all GRP solvers require a classical Riemann solver, see [22]; to this end we adopt the Dumbser-Osher-Toro (DOT) scheme [10], modified as described in [27]. The numerical scheme is implemented using a local time stepping second order implementation [25] which ensures a consistent high-order treatment of coupling conditions at junctions of viscoelastic vessels [24, 26]. For background on the ADER approach and recent developments see [36, Chapters 19 and 20] and references therein.

The one-dimensional domain, at terminal sites, is coupled to lumped parameter models representing the peripheral circulation (see [12] and therein cited references for full details). For the network considered here, see [1], these models are purely resistive

$$Q = \frac{P_{1D} - P_{out}}{R_{TOT}}\,, \tag{11}$$

where Q is the flow rate across the lumped model, P_{1D} is the pressure in the one-dimensional domain, P_{out} is the outlet pressure and R_{TOT} is the total peripheral resistance.

We conclude this section by noting that more complex terminal models can be used, as those that include the compliance of peripheral vessels and/or the inertia of blood in those networks. In such cases the terminal models are ordinary differential equations that have to be coupled to the one-dimensional domain. Moreover, it is worth mentioning that other portions of the cardiovascular system can also be modeled using lumped models, e.g. the heart, the pulmonary circulation and valves in veins (see, e.g., [28, 29]).

2.2 The Kalman filter for parameter estimation

The Kalman filter is a widely used tool for data assimilation application, aiming at improving the results of a computational model and estimate the values of unknown parameters, taking into account available measurements on a given system [20, 3, 32].

In order to introduce the method from a general point of view, let us write the discretized evolution of the one-dimensional model described in Section 2.1 in the form of a dynamical system

$$\begin{aligned} X_{n+1} &= \mathscr{F}(X_n, \theta)\,, \\ X_0 &= Y + \xi^X\,, \end{aligned} \tag{12}$$

where X_n denotes the ensemble of the *state variables* at time step t_n (values of flow, pressure and cross-sectional area at each discretization node along the network and state variables of the lumped parameter models), $\mathscr{F}$ is an operator which depends on equations (6) and (11) and on their particular discretization, and θ is a vector of *parameters*, whose values are to be estimated. For instance, these unknown parameters might comprise the Young's modulus of selected vessel segments or the terminal resistances of lumped parameter models. Finally, Y stands for the initial condition, while ξ^X is a random variable that takes into account the uncertainty of the initial state.

Let us now assume that a measurement vector $Z_n \in \mathbb{R}^M$, for M measurements, is available at $n = 1, \dots, N$ selected time instants, obtained by observing the state X through an *observation* operator $\mathscr{H}(X_n)$, such that

$$Z_n = \mathscr{H}(X_n) + \xi^Z\,,$$

affected by a noise ξ^Z, which is usually assumed to be independent at all times and Gaussian with zero-mean and covariance matrix Σ^Z. In a clinical setting, the main contribution to the observation noise is given by error statistics of measurement devices, thus the noise distribution of the observation will be considered constant in time [32]. For the ease of presentation, we assume that measurements Z are available at each discrete time instant t_n for which a numerical approximation of blood flow dynamics is resolved. In practice, this assumption can be easily relaxed interpolating the available observations at the discrete simulation times.

The idea behind the Kalman filter is to apply a prediction-correction scheme to an augmented state (X_n, θ_n), including a trivial dynamics for the parameters (assuming that they do not change in time).

Namely, the prediction is obtained via a forward propagation

$$\begin{aligned} X^-_{n+1} &= \mathscr{F}(X^+_n, \theta_n)\,, \\ \theta^-_{n+1} &= \theta_n\,, \end{aligned} \tag{13}$$

while the correction takes into account the discrepancies between observations and measurements (often called *innovation*)

$$\begin{aligned} X^+_{n+1} &= X^-_{n+1} + K_X\left(Z_n - \mathscr{H}(X^-_{n+1})\right)\,, \\ \theta^+_{n+1} &= \theta^-_{n+1} + K_\theta\left(Z_n - \mathscr{H}(X^-_{n+1})\right)\,. \end{aligned} \tag{14}$$

The *Kalman matrices* K_X and K_θ are defined in order to minimize the distance between observations and measurements in a proper norm, which depends on the confidences in both the measures and the model.

2.2.1 The reduced-order unscented Kalman filter

It can be shown that, in the case of linear dynamics with white noise, the Kalman filter provides an optimal estimate [20]. For non-linear systems, different extensions of the Kalman filter are available. Among these, the unscented Kalman filter achieves second order accuracy employing a minimal set of deterministically chosen points in the state space for forward propagation [39].

In this case, the prediction-correction strategy for the filtering consists in (i) a forward propagation of the mean (current estimate) and covariance of the state, based on the dynamics of selected points in the state space, and in (ii) a correction of the propagated statistics, computed taking into account the noisy observations. In particular, the UKF computes state and parameter estimates at all time iterations, as well as state and parameter covariance matrices, based on the current confidence, represented by the covariance matrix P^X and by the observation error covariance P^Z.

The main drawback of the UKF is that it might require costly matrix operations (factorization and computation of inverse matrices) on large matrices (dimension of the state vector). However, neglecting the uncertainty on the state (i.e. on the initial conditions) allows to formulate the so-called *reduced-order* unscented Kalman filter (ROUKF) [20], for which the filtering operations only involve matrices of the size of the unknown parameter space, which is typically much lower than the size of the state space. Moreover, it can be shown that for the estimation of p parameters, only a discretization of $p+1$ points for the state-parameter space is required. This optimal sampling can be obtained using simplex sigma-points $\left(I_{(i)}\right)_{i=1,\dots,p+1}$ ($p+1$ vectors of size p) with properly defined weights $d_1,\dots,d_{p+1}$. For simplicity of notation, in what follows the sigma-points will be grouped in a matrix $\mathscr{I}$ (of size $(p+1)\times p$), while the weights will be collected in a diagonal matrix D. In practice, the sigma-points and their weights can be recursively defined for each size of the parameter space. We refer to [20, 15] for details.

The algorithm The ROUKF algorithm can be summarized as follows (see, e.g., [20, 3] for further details):

- Initialization: Assume that an initial parameter covariance matrix P^θ and the error covariance matrix P^Z, as well as the initial estimates X_0^+ and θ_0^+, are given. In the simulations presented in the following section, we will assume that the matrices P^θ and P^Z are diagonal matrices with entries $\left(\sigma^2_{\text{param},i}\right)_{i=1,\dots,p}$ and $\left(\sigma^2_{\text{obs},j}\right)_{j=1,\dots,M}$, respectively. In practice, the constants σ^2_{param} control the confidence on the initial parameter estimate, while σ^2_{obs} can be interpreted as the confidence on the accuracy of the measurements. Set $n=0$ and:
$$L^\theta = \mathbb{I},\ L^X = 0, U_0 = \left(P^\theta\right)^{-1}.$$
- Until convergence, do
  - Sampling:
$$C_n = \sqrt{U_n^{-1}} \quad \text{(Cholesky factorization)}$$
$$X^+_{n,(i)} = X^+_n + L^X_n C^T_n I_{(i)},\ i=1,\dots,p+1$$
$$\theta^+_{n,(i)} = \theta^+_n + L^\theta_n C^T_n I_{(i)},\ i=1,\dots,p+1$$

- Forward propagation:

$$
\begin{aligned}
X^-_{n+1,(i)} &= \mathscr{F}(X^+_{n,(i)}, \theta_{n,(i)}), i = 1, \dots, p+1 \\
\theta^-_{n+1,(i)} &= \theta^+_{n,(i)}, i = 1, \dots, p+1 \\
X^-_{n+1} &= \mathbb{E}\left[X^-_{n+1,(1,\dots,p+1)}\right] \\
\theta^-_{n+1} &= \mathbb{E}\left[\theta^-_{n+1,(1,\dots,p+1)}\right]
\end{aligned}
$$

- Compute innovation:

$$\Gamma_{n+1} = Z_{n+1} - \mathscr{H}(X^-_{n+1})$$

- Update covariances:

$$
\begin{aligned}
L^X_{n+1} &= X^-_{n+1} D \mathscr{J}^T \\
L^\theta_{n+1} &= \theta^-_{n+1} D \mathscr{J}^T \\
L^\Gamma_{n+1} &= \Gamma^-_{n+1} D \mathscr{J}^T \\
U_{n+1} &= \mathscr{J} D \mathscr{J}^T + \left(L^\Gamma_{n+1}\right)^T P^Z L^\Gamma_{n+1}
\end{aligned}
$$

- Correction:

$$
\begin{aligned}
X^+_{n+1} &= X^-_{n+1} - L^X_{n+1} U^{-1}_{n+1} \left(L^\Gamma_{n+1}\right)^T P^Z \mathbb{E}\left[\Gamma_{n+1}\right] \\
\theta^+_{n+1} &= \theta^-_{n+1} - L^\theta_{n+1} U^{-1}_{n+1} \left(L^\Gamma_{n+1}\right)^T P^Z .
\end{aligned}
$$

- Set $n = n+1$.

The stopping criterion was defined averaging the estimated parameters over each cardiac cycle, and monitoring their RMS deviation.

2.2.2 Renormalization of measurement data

For the application of the Kalman filter, in order to compare the results obtained using measurements of different nature (i.e., flow rates and pressures), the errors between the measurements and the observations are renormalized when computing the innovation. Namely, when considering pressure data, the errors are rescaled by the average pressure value over a cycle, while, in the case of flow measurements, the errors are renormalized using the maximum (absolute) value of flow.

2.2.3 Filter parameters

The algorithm described in Section 2.2.1 depends on two sets of user defined parameters, denoted by σ^2_{param} and σ^2_{obs}, corresponding to a p-dimensional and M-dimensional arrays, respectively. The vector σ^2_{param}, defining the initial parameter covariance, determines in practice the width of the initial sampling for the sigma-points, i.e., how much the particles will differ from the initial condition. In our experience, this aspect might lead to stability issues in the case of estimating several parameters (which yields a larger sigma-point sample), if the initial parameter covariance is chosen too large. Especially in the presence of non-linearities, as

the sampling does not uniformly affect the state and the parameters of the model, an excessive sampling step might give rise to (non-physical) spatial and temporal discontinuities in the model, which cannot always be handled numerically.

The array of parameters σ^2_{obs} is theoretically related to the level of confidence of each measurement, and, it depends on the intensity of noise. In practice, σ^2_{obs} influences both the sampling and the correction step (through the matrices U and $P^{\mathbf{Z}}$). Ideally (in the linear case), if the measurements are noise-free, large values of σ^2_{obs} might provide fast convergence towards the exact parameter. However, we observed that large values of σ^2_{obs} might yield stability problems, especially in the initial phase of the filter, due to the discontinuities which might be introduced by the filter during the correction and sampling steps.

A further variable, which plays a relevant role in our numerical tests, is the filter time step Δt_F, i.e., the time interval between two correction steps. In fact, when using a limited number of measurements (e.g. observation located at midpoints of vessels), Δt_F is related to the covariance between parameters and measures. This aspect might become particularly important if the observed vessels are far from the sought parameters, as, after correcting the parameter, the information needs a certain amount of time to reach the observed location. On the other hand, increasing the filter time step reduces the number of corrections, but may result in a slower convergence.

In practice, in order to define the parameters, we consider the following approach:

- Assuming that no a priori information is available concerning the parameters, the initial covariances will be taken all equal. The value of the covariances will be smaller (order of 10^{-2}) when a large number of parameters has to be estimated, and larger (order of 10^{-1}) when estimating few parameters.
- Independently of the number of available measurements, the initial measure covariances will be defined equal for all measures as

$$\sigma^2_{\text{obs},i} = \gamma \frac{\Delta t_F}{T_0},\ i = 1, \ldots, M \tag{15}$$

  where T_0 is the length of the cardiac cycle, and γ is a free parameter. With this definition, the parameters $\sigma^2_{\text{obs},i}$ take into account the fact that, varying Δt_F, also the number of filter correction steps changes.

2.3 Identifiability analysis

Given a dynamical system and a set of uncertain parameters, the goal of identifiability analysis is to understand which parameters can be more robustly estimated, whether there might be difficulties in the estimation and in which case additional measurements could improve the results.

2.3.1 Traditional sensitivity

One possible approach consists in considering the *sensitivity* of the observed system to parameter changes, i.e. how measurements are sensitive to small perturbations in the value of

parameters. Formally, let p be the number of uncertain parameters. The sensitivity can be quantified by the matrices (of size $p \times M$)

$$S_k^j(t_n, \theta_0) = \frac{\hat{\theta}_{0,k}}{\hat{h}_j} \frac{\partial \mathscr{H}_j(X_n)}{\partial \theta_k}|_{\theta_{0,k}}, \text{ with } j = 1, \dots, M,\ k = 1, \dots, p, \tag{16}$$

defined at each time step t_n for a p-dimensional element θ_0 in the parameter space, given, e.g., by available initial estimates or reference values of the parameters of interest. Notice that, in definition (16), the observations and parameters are rescaled by reference values $(\hat{h}_j)$ and $(\hat{\theta}_{0,k})$, in order to obtain a non-dimensional sensitivity (necessary when comparing different types of parameters and different types of measures).

The relative magnitudes of the total system sensitivity with respect to parameters might be used to characterize their identifiability over time. In particular, small sensitivity values (for a certain time-interval) imply that the observed quantities are weakly sensitive to parameters. In this case, the observations might not contain sufficient information about the parameters, hence leading to potential identifiability complications [35]. It is worth noticing that the sensitivity matrix (16) characterizes the observation in terms of changes in *single* parameters, in order to quantify the identifiability of parameters. However, this does not provide any information about the correlation between parameters and how the identifiability would change enlarging or reducing the set of parameters to be estimated.

2.3.2 Fischer information matrix

For time dependent problems, additional information about the parameter sensitivities is provided by a cumulative Fischer information matrix for the set of measures, defined, for the whole time interval, by the $p \times p$ matrix

$$\mathscr{M} = \sum_{i=1}^{N} \sum_{j=1}^{M} \frac{1}{\sigma_j^2(t_i)} S^j(t_i, \theta_0) \left(S^j(t_i, \theta_0)\right)^T \tag{17}$$

where N and M stand for the total number of time steps (at which the measurements are available) and the total number of measurements, respectively, and $S^j(t_i, \theta_0)$ is the j-th column of the sensitivity matrix (16) calculated at time t_i at a given point θ_0 of the parameter space. Moreover, the weight $\sigma_j^2(t_i)$ is the confidence on the j-th measure at time t_i.

In practice, with respect to the traditional sensitivity matrix, the matrix $\mathscr{M}$ provides not only information about the sensitivity of each parameter (diagonal elements), but it quantifies also the correlation between them (off-diagonal entries), according to the available measurements.

2.3.3 Generalized sensitivity function

An extension of the traditional sensitivity is represented by the so-called generalized sensitivity function (GSF) [32, 35] which aims at characterizing the sensitivity of the parameter estimations with respect to the available measurements. Moreover, the GSF quantifies how the information content of the measurements with respect to individual parameters is distributed during the experiment, providing also insight into the degree of correlation between model parameters. We refer, e.g., to [35] for a detailed derivation. At each time step t_n (for

which measurements are available), the GSF is a p-dimensional vector whose components are defined by

$$g_k(t_n) = \sum_{i=1}^{n} \sum_{j=1}^{M} \left(\frac{1}{\sigma_j^2(t_i)} \left(\mathscr{M}^{-1} S^j(t_i, \theta_0) \right)_k S^j(t_i, \theta_0)_k \right), \; k = 1, \ldots, p. \tag{18}$$

Notice that, if the parameters are strongly uncorrelated (i.e., $\mathscr{M}$ is strongly diagonal dominant), each component of the GSF (18) can be seen as a weighted norm of the columns of the traditional sensitivity. In this case, the largest components of the GSF also correspond to the parameters with highest sensitivity. In general, the following information about parameter identifiability can be drawn from the profile of the GSFs over time: (i) sharp increase in GSFs implies high concentration of parameter information (in the corresponding time interval); (ii) monotone non-decreasing GSFs imply that parameters are uncorrelated; (iii) large oscillations in GSFs imply large correlation between parameters, and hence potential identifiability problems [32, 35].

Hence the GSF can be used, on the one hand, to preprocess the system in order to understand whether a specific set of parameters might suffer from identifiability problems, and, on the other hand, to decide whether the set of measures is sufficient for the estimation, and, if not, whether including additional observations could be helpful. At the same time, together with the Fischer information matrix, the GSF provides information about sensitivity and correlation of parameters, allowing to decide – given the set of observations – whether to exclude one or more parameters from the estimation algorithm. However, it is important to note that the traditional sensitivity matrix (and therefore the GSF) can, in general, only be computed in silico (i.e. computing the sensitivity matrix numerically from synthetic data, observing the numerical results when varying the parameters), and an evaluation of the sensitivity based on real measurements is not feasible a priori. As a consequence, in realistic situations, a GSF which reveals no identifiability issues according to the above criteria (i)–(iii) does not necessarily imply that the parameters will be correctly estimated.

2.4 An in vitro arterial model

For this study, we consider the in vitro model of the human arterial network described in [19, 1]. Figure 1 shows the vessel network, which is composed of 37 silicone tubes. The network inlet is connected to a pump, mimicking the action of the heart, while terminal vessels are coupled to purely resistive elements, i.e., using the lumped parameter model defined by (11).

This model has been extensively used for validation of numerical approaches (see, e.g., [1, 27]) and to compare results obtained by different numerical methods [7]. Here we use this model because it offers the possibility of assessing the Kalman filter in a realistic – but still highly controlled – in vitro setting. In fact, the uncertainty on model parameters is very low as mechanical and geometrical properties of the vessels that compose the network were carefully measured and reported in the above cited references. Moreover, experimentally measured flows and pressures at different locations, with a relatively detailed sampling (about 800 time instants per cardiac cycle), are available [7][1]. It is worth noting that for this network, the

[1] The measurement data have been kindly provided by Dr. J. Alastruey and have recently been made available as supplementary material in [7].

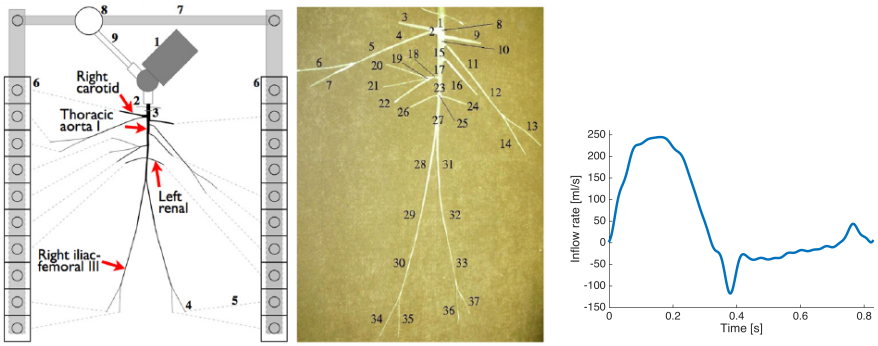

Figure 1: Schematic representation of the in vitro model of the human arterial network presented in [19, 1] (left, center), reproduced with permission. Inflow boundary condition for vessel 1 (right).

numerical method, which is based on an explicit local time stepping second-order finite volume scheme [25], needs approximately one second of wall clock time to solve a cycle using OpenMP parallel computing on a Intel® Xeon® CPU E5-2650 v2 @ 2.60GHz processor.

2.5 Tests setup and evaluation

We will present two setups in order to explore the capability of the Kalman filter to estimate parameters in the above described in vitro setting. First, we investigate the estimation of *terminal resistances*, i.e., the parameters defining the 0D boundary conditions (11). This case study is chosen since terminal resistances are normally hard to estimate, and a rather standard procedure is to assign their values in order to approximate given flow distribution pattern and mean pressure. Hence, being able to estimate the resistances based on few measurements clearly represents an improvement in the setting of a patient-specific simulation. Next, we focus on the *arterial wall properties*, considering the estimation of Young's modulus and wall thickness of vessels. In this case, the estimation of these parameters is mainly motivated by the fact that, unlike geometrical information, they can hardly be retrieved from medical images.

In the different tests, we will present estimation results obtained either with *synthetic measurements*, i.e. observation obtained directly from the numerical model (possibly perturbed with white noise) and with experimental measurements.

Furthermore, two different errors will be monitored. On the one hand, we consider the discrepancy between the estimated parameter and the reference parameter provided in [1]. On the other hand, since the scope of the Kalman filter is to minimize a given functional, depending on the difference between numerical results and provided measurements, we will also consider the quantity

$$e_i = \sqrt{\frac{1}{N}\sum_{n=1}^{N}\left(\frac{\mathscr{H}_i(\tilde{X}_n) - Z_{i,n}}{\hat{Z}_i}\right)^2}, \tag{19}$$

corresponding to the RMS deviation between the measurements and the observations obtained when running the forward model with the estimated parameters for the i-th measurement. In (19), N denotes the number of time steps per cardiac cycle, while Z_i stands for the

time-series of the i-th measurement ($Z_{i,n}$ is the i-th measurement at time t_n) and $\tilde{X}$ is the state vector obtained with the estimated parameters. Furthermore, the normalization factor $\hat{Z}_i$ corresponds to the time average over a period (in the case of pressure measurements) or to the maximum value (in the case of flow rate measurement), consistently with the renormalization introduced in the Kalman filter for the i-th measurement time series (see Section 2.2.2).

3 Estimation of terminal resistances

Here we focus on the estimation of parameters that define 0D boundary conditions for the mathematical model. This aspect has been recently investigated to assess the performance of the ROUKF in 1D-0D models with in silico measurements [18] and in the context of calibrating 3-parameters (Windkessel) boundary condition models for 3D simulations (e.g., [3, 32]). Notice, however, that in the present arterial network model, due to the experimental setup, boundary conditions are purely resistive (one parameter per terminal vessel).

This test aims at investigating whether observations (mainly near the terminal branches) allow accurate estimates of terminal resistances, and, if so, how robust the resulting estimation is (e.g., with respect to noisy data and/or how the estimate differs using synthetic or experimental data). We consider two situations: first the joint estimation of all terminal resistances, in order to assess the robustness of the filter against a large number of uncertain parameters; next, we focus on a single terminal branch, in order to study more closely how the estimation might be affected by the lack of accurate measurements close to the terminals.

3.1 Estimation of multiple terminal resistances

The in vitro model contains 16 terminal resistances (see Figure 1), whose vessel indices and reference values (given in [1]) are summarized in Table 1.

Vessel	3*	6	7*	9	13*	14*	16	20*
R_{ref} [10^9Pa s m^{-3}]	2.67	3.92	3.24	3.11	3.74	3.77	2.59	3.54

Vessel	21	22	24*	26	34*	35*	36	37
R_{ref} [10^9Pa s m^{-3}]	4.24	3.75	3.46	3.45	5.16	5.65	4.59	3.16

Table 1: The indices of the terminal vessels (top rows) with the corresponding values of reference resistances (bottom rows). Additionally, the star indicates the branches where flow measurements are available (either located on a terminal vessel or on neighboring ones).

In order to restrict the estimated parameters to positive values, we parametrize the value of the i-th terminal resistance as $R_i = R_{i,\text{ref}} 2^{\theta_i}$, where $R_{i,\text{ref}}$ is the reference value [1], so that for $\theta_i = 0$, the estimated value corresponds to the reference parameters. This parameterization holds for all tests presented in this work.

As initial condition, we randomly choose the (non-dimensional) parameters θ_i between -2 and 2. Then, we run the one-dimensional model for the in vitro setting until a periodic regime is reached, in order to generate an initial state (to be used to start the Kalman filter) compatible with the initial guesses of the parameters. An initial parameter covariance of $\sigma^2_{\text{param}} = 0.01$ was used, while $\gamma = 10^4$ was selected for the measure covariances. Moreover, the filter was

applied with a time step $\Delta t_F = 0.01$ for a simulation time of 300 s (corresponding to about 363 cardiac cycles of period 0.827 s). The required computational time was of about 20 minutes.

For the estimation of these parameters, we consider the measurements that are available at the terminal vessels (3, 7, 14, 20, 24, 34) and the measurements on vessels 11, 29 and 30, which are located close to three terminal bifurcations. Each measurement corresponds to one datum per vessel, assumed to be acquired at the middle point.

In what follows, we compare the results of the estimation algorithm in two cases:

- in silico: feeding the filter with synthetic measurements, i.e., the numerical results of the one-dimensional model with the reference parameters, perturbed with Gaussian noise, and
- in vitro: employing the available experimental measurements.

In both cases, we first perform an identifiability analysis for the considered setting (16 terminal parameters to be estimated and 9 observations) based on the Fischer information matrix and on the GSF.

3.1.1 Estimation using flow measurements

From the Fischer information matrix (Figure 2, left), one can clearly distinguish the terminals corresponding to measured flows (the darkest diagonal entries, with a lower correlation level and hence a higher sensitivity), as well as the couple of terminals corresponding to the same bifurcation (darker 2×2 blocks along the diagonal). On the other hand, blocks with similar grey tone (e.g. vessel 6 and the branches 21-22 and 36–37) indicate that parameters are correlated and hence that potential identifiability problems can occur. Similar conclusions can be drawn

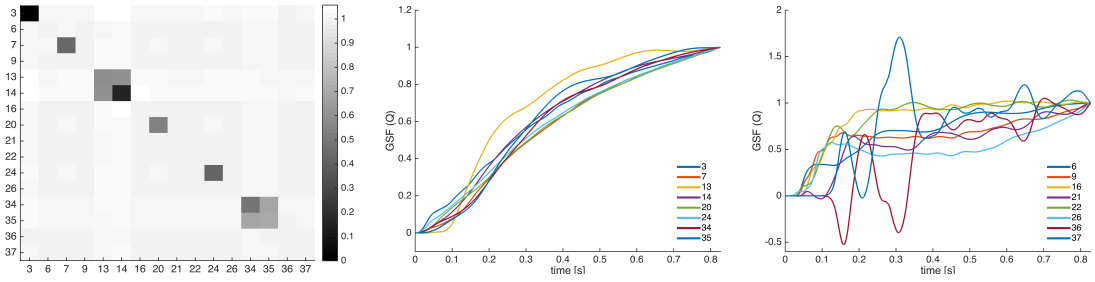

Figure 2: Left: the Fischer information matrix for the set of terminal parameters and considering flow measurements on vessels 3, 7, 11, 14, 20, 24, 29, 30, and 34; the linear greyscale goes from black (highest value) to white (lowest value). Right: the GSF for the terminal parameters and the considered flow measurements; for clarity, the most and less oscillatory components are shown separately.

observing the profile of the GSF in time (Figure 2, right). In fact, one can easily recognize two types of behavior. First, we observe a monotone increasing GSF for vessels 3, 7, 13, 14, 20, 24, 34 and 35, with small oscillations present only for vessels 13 and 16. These vessels correspond to the branches where measurements are available, with the exception of vessel 16, which, however, is a single-branch terminal and therefore possibly less correlated with other

parameters. The GSFs of the remaining vessels (6, 9, 21, 22, 26, 36, 37) are characterized by an oscillatory behavior, where an underlying monotone increase is only visible for vessels 6 (a measurement is available on vessel 7) and 9 (single-branch terminal).

The estimates resulting from the Kalman filter are shown in Figure 3, confirming the expectations derived from the identifiability analysis. In particular, when in silico data is used, one clearly sees that parameters characterized by a *favorable* GSFs (Figure 2, middle) are also better estimated, reaching values which are very close to the reference ones. On the contrary, the filter delivers poor estimates for the parameters whose GSFs have oscillating profiles (error between 20% and 30% for terminals 6, 9, 16, 21, 22, 26, 36 and 37).

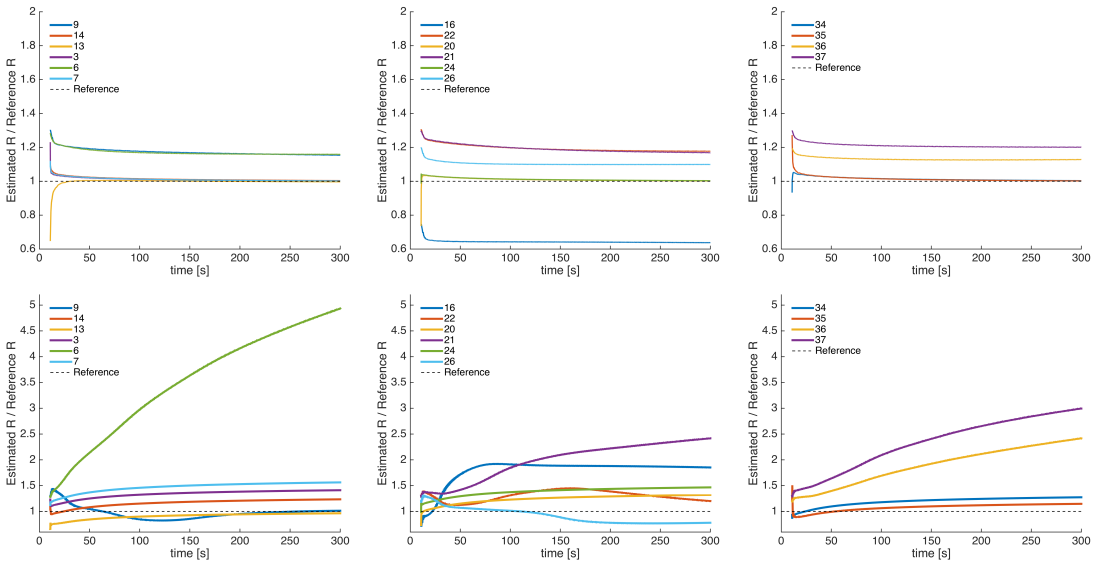

Figure 3: Estimated terminal resistances (with flow measurements), dividing upper (left), middle (center) and lower (right) body. The continuous line shows the estimated value over time (divided by the corresponding reference values, so that 1 corresponds to the reference resistance [1]). Top: Synthetic measuremets. Bottom: Experimental measurements.

The identifiability difficulties are more visible using experimental measurements. In this case, the estimates for some of the terminal resistances with oscillating GSF tend to diverge from the reference value (terminal 6, 21, 36 and 37), while in the other cases, when the estimation converges, the relative error with respect to the reference parameter is close to 50% (terminals 9, 16 and 26). For the remaining parameters, values relatively close to the reference ones (with an error of about 30%) are obtained. Hence, in general, less accurate estimation than the in silico case is achieved. Also, the filter based on synthetic data needs less time to converge (unless the estimates diverge). This is expected, and it is in line with the better conditioning of the problem when using model-derived synthetic data.

Remark 1. *Notice that, even in the in silico case, where the reference parameters minimize the error with respect to the observations, the final estimates are rather different from the reference values (up to 30% of error). This result might depend on the number of parameters estimated at the same time (with a small set of measures). In fact, in this case, the sigma-point sampling can spread the particles relatively far in the parameter space, making it difficult for the filter to retrieve the correct solution.*

Finally, we monitor the errors (19) with respect to the experimental measurements obtained running the one-dimensional model with the estimated parameters. This is important in order to assess the outcome of the filter. In fact, in the in vitro case, although the estimated parameters might differ from the reference values, the estimation results should allow to decrease the discrepancies between data and observations. These errors are summarized in Figure 4, considering the forward simulations with the initial parameters, the reference values and the new estimates. In this figure we show errors for all vessels for which measurements are available, including thus not only measurements used for the estimation, but all available information. One can see that, in all cases, the solution obtained using the estimated parameters always features the smallest errors (errors for vessels denoted with grey bars). However, the negative impact of the estimated parameters on other errors, especially for pressure, invalidates the results of the estimation process. In fact, it is observed that, regardless the flow measurement was available or not, there are very large discrepancies in the values of the pressure in all vessels. In fact, since only flow measurements are used, the estimation process has no control on pressure levels and this can clearly lead to an invalid estimation (see Figure 4 right).

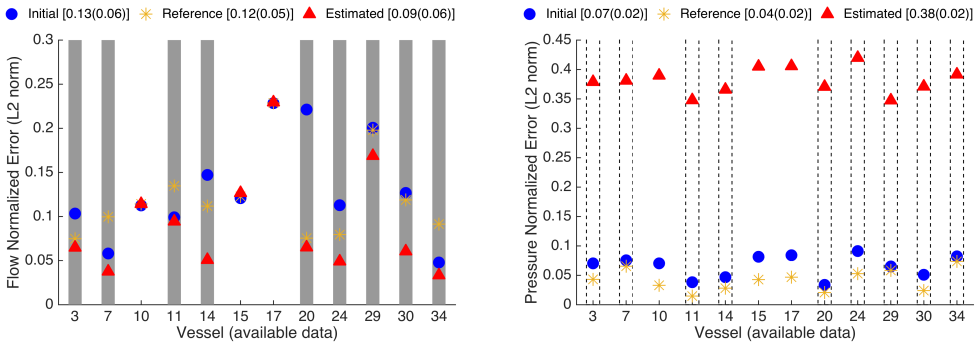

Figure 4: Summary of the errors obtained running the one-dimensional model with the initial values of the resistances (blue), with the reference values (yellow) and with the estimated parameters (red), in the case of flow data. The x-axis indicates the observed vessel, while the y-axis shows the corresponding error. Errors average (standard deviation) are shown for each model setting in the legends. Left: errors with respect to flow data. Right: errors with respect to pressure data. Grey bars denote vessels for which measurements of the quantity for which the error is computed have been used in the estimation, whereas dashed lines indicate vessels for which a measurement of the other quantity has been used for the estimation. For example, a vessel with dashed lines in the pressure error plot indicates that the flow measurement in this vessel was used for the estimation.

3.1.2 Estimation using pressure measurements

Figure 5 shows the Fisher information matrix (left) and the GSF (middle and right) for the case in which pressure measurements are used. For the sake of clarity, the GSFs are divided in two plots as in the previous Figure 2. However, unlike the case of flow measurement, one can see a higher correlation between parameters and more complex GSF profiles, which reveals a less overall sensitivity of the pressure measurements to the terminal resistances. In particular, in

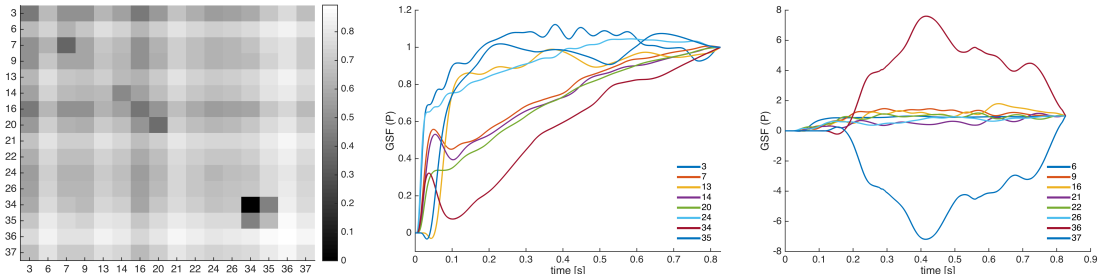

Figure 5: Left. The Fischer information matrix for the set of terminal parameters considering pressure measurements on vessels 3, 7, 11, 14, 20, 24, 29, 30, and 34; the linear greyscale goes from black (highest value) to white (lowest value). Right: The GSF for the terminal parameters and the considered pressure measurements.

this case it is rather difficult to distinguish between more and less identifiable parameters, as all GSFs are mainly monotone, but affected by small amplitude oscillations (with the exception of vessels 36 and 37, showing very large oscillations). Moreover, the behavior of the GSFs varies during the cardiac cycle, due to the fact that the information contained in the measurements is not uniformly distributed over time. Hence, one can conclude that all the parameters (except vessels 36 and 37) can be estimated using pressure measurements, but, at the same time, that the quality of the estimation might be worse than in the case of flow measurements, due to the high correlation between terminal resistances.

The estimation results confirm to some extent these expectations. In the in silico case (Figure 6, top), all terminal resistances are estimated in relatively short time (between 100 and 200 cardiac cycles), with final errors less than 20% in several cases. The only exceptions are the terminal resistances on vessels 13, 16, 21, 22 and 37 (with errors of up to 40%).

As for the case of experimental flow measurements, also in the case of in vitro pressure data several potential identifiability issues emerge. As in the case in which experimental flow measurements were used, several parameters do not reach a stationary state after more than 300 cardiac cycles. For the converged parameters, the difference with respect to reference values stays around 20%, besides for vessels 13 and 16 (errors of 40%). The remaining parameters, whose estimates do not reach a steady value, show errors above 50%. However, unlike in the case of flow measurements, the maximum error is of the order of 60% for terminal 35 (against the 500% error of terminal 6 estimated with flow observations).

Finally, we monitor the errors (19) with respect to the experimental measurements obtained running the one-dimensional model with the estimated parameters (Figure 7). In most of the cases the new estimates result in smaller errors, or errors comparable with the ones obtained using the reference values. Only for the observation in vessel 24, the error corresponding to reference parameters is below the one obtained with the new set (0.06 against 0.075). This aspect could be a consequence of the higher correlation (hence less sensitivity) of terminal resistances when using pressure measurements (Figure 5), combined with the large number of parameters to be estimated, resulting in a harder (worse conditioned) minimization problem to be solved by the filter.

Considering errors with respect to flow measurements, we see that, as for the case of the estimation performed using flow measurements, the impact of the estimation process on errors

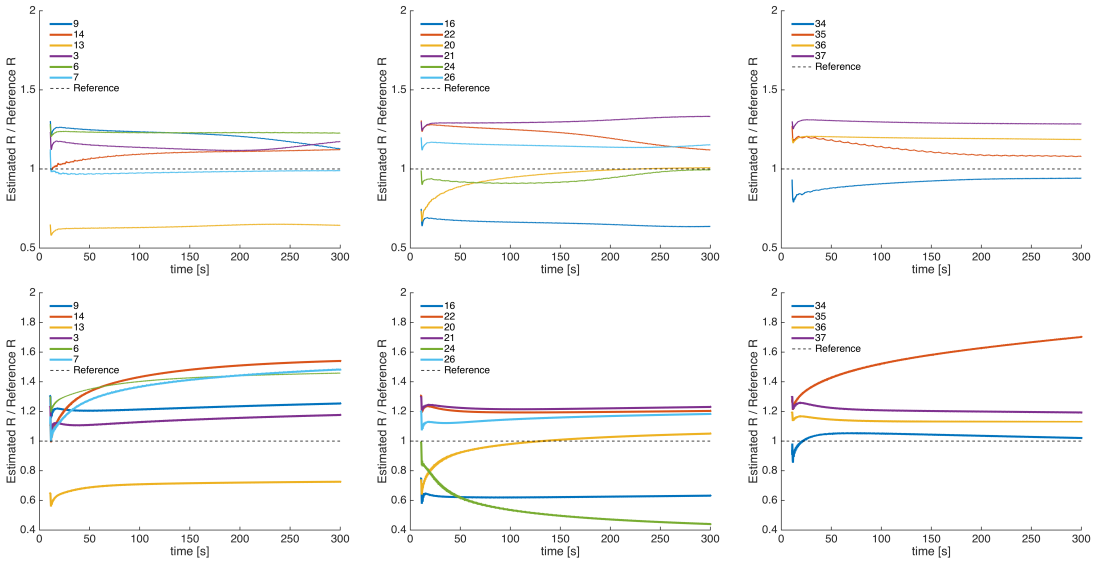

Figure 6: Estimated terminal resistances (with pressure measurements), dividing upper (left), middle (center) and lower (right) body. The continuous line shows the estimated value over time (divided by the corresponding reference values, so that 1 corresponds to the reference resistance [1]). Top: Synthetic measurements. Bottom: Experimental measurements.

for non-monitored quantities is negative, with errors for flow measurements greater than the ones obtained using initial guesses for parameters.

This aspect could be a consequence of the higher correlation (hence less sensitivity) of terminal resistances when using pressure measurements (Figure 5), combined with the large number of parameters to be estimated, resulting in a more difficult (worse conditioned) minimization problem to be solved by the filter.

3.1.3 Estimation combining flow and pressure measurements

Based on the previous results, we performed the estimation of terminal resistances using flow and pressure measurements. First we considered all flow and pressure measurements used in Sections 3.1.1 and 3.1.2. Figure 8 shows the progress of the estimation procedure for synthetic (top row) and experimental data (bottom row). It is evident that using a combination of pressure and flow measurements has a positive impact on the velocity by which the parameters converge to a given value and on the agreement of the estimated parameters with reference values. In fact, acceptable estimates for almost all parameters are reached after 100 cardiac cycles, for both, synthetic and experimental measurements. Moreover, in the case of synthetic measurements final errors are of less than 50% of the reference values, whereas for experimental measurements errors are below 60% of the reference values. The better performance of the filter in this setting is also seen when one evaluates errors of forward simulations performed with estimated parameters, as shown in Figure 9 (top row). In fact errors are smaller than or similar to the ones obtained with reference parameters for both quantities, flow and pressure. These results show that mixing flow and pressure measurements is beneficial for the estimation of terminal resistances. However, it is unrealistic to assume that pressure mea-

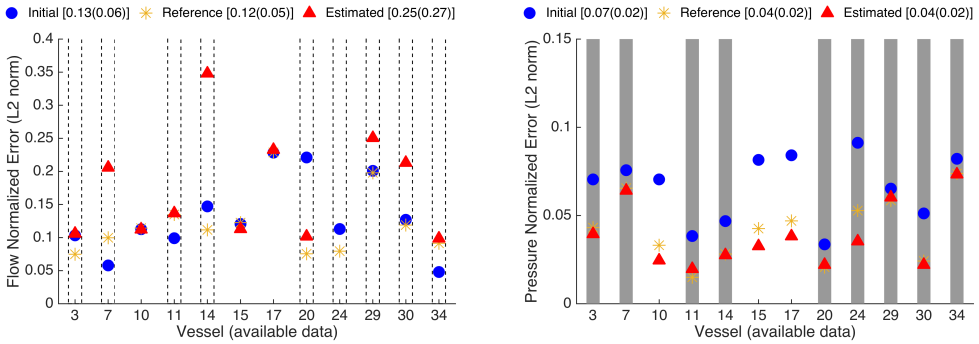

Figure 7: Summary of the errors obtained running the one-dimensional model with the initial values of the resistances (blue), with the reference values (yellow) and with the estimated parameters (red), in the case of pressure data. The x-axis indicates the observed vessel, while the y-axis shows the corresponding error. Errors average (standard deviation) are shown for each model setting in the legends. Left: errors with respect to flow data. Right: errors with respect to pressure data. Grey bars denote vessels for which measurements of the quantity for which the error is computed have been used in the estimation, whereas dashed lines indicate vessels for which a measurement of the other quantity has been used for the estimation. For example, a vessel with dashed lines in the flow error plot indicates that the pressure measurement in this vessel was used for the estimation.

surements at several locations can be obtained from standard clinical monitoring procedures. It is thus advisable to assess how the filter behaves in the case of using flow measurements, which can be obtained with non-invasive procedures, and a single pressure measurement. We have performed two tests, taking all flow measurements used in Section 3.1.1 and a single pressure measurement. Moreover, we have performed the estimation using a peripheral pressure measurement location (vessel 7, corresponding to the right ulnar artery) and a central location (vessel 10, corresponding to the aortic arch). For the sake of brevity, only errors of forward simulations are displayed. Figure 9 shows results for the case of a single pressure measurement in the ulnar artery (middle row) and in the aortic arch (bottom row). It can be seen that using a single pressure measurement, in combination with flow measurements, is almost as beneficial as using many pressure measurements.

Furthermore, it is observed that the errors in the estimation of the flow are insensitive to the location of the pressure measurement. Nevertheless, the errors in the pressure are sensitive to the place where pressure is being monitored. This can be considered an expected result, in fact, monitoring the pressure at central locations provides different systemic information than the peripheral pressure. Remarkably, the errors in the pressure are smaller when considering the measurement at the central location.

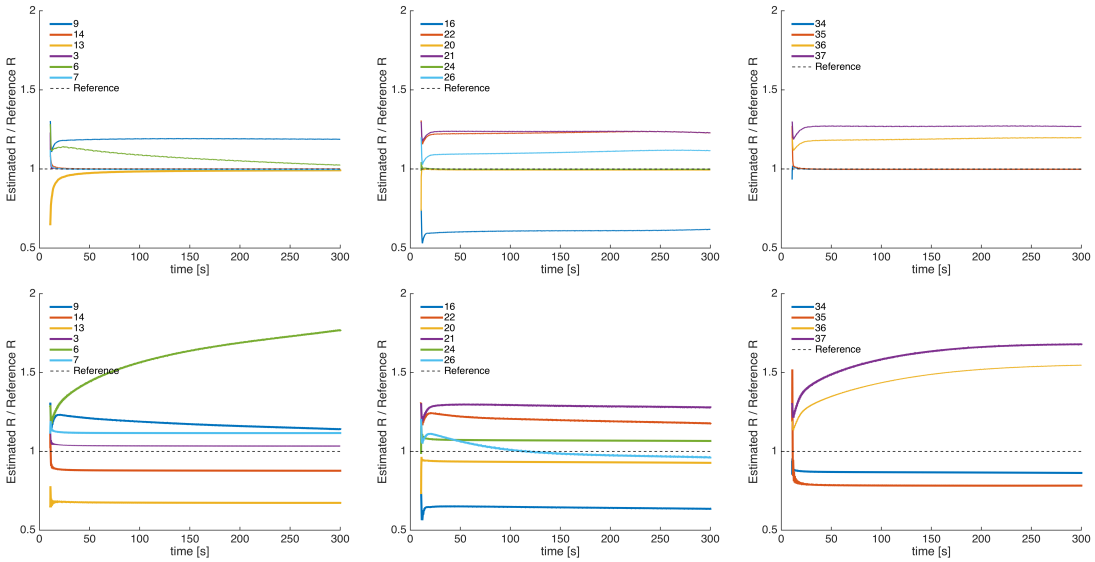

Figure 8: Estimated terminal resistances (combining flow and pressure measurements), dividing upper (left), middle (center) and lower (right) body. The continuous line shows the estimated value over time (divided by the corresponding reference values, so that 1 corresponds to the reference resistance [1]). Top: Synthetic measurements. Bottom: Experimental measurements.

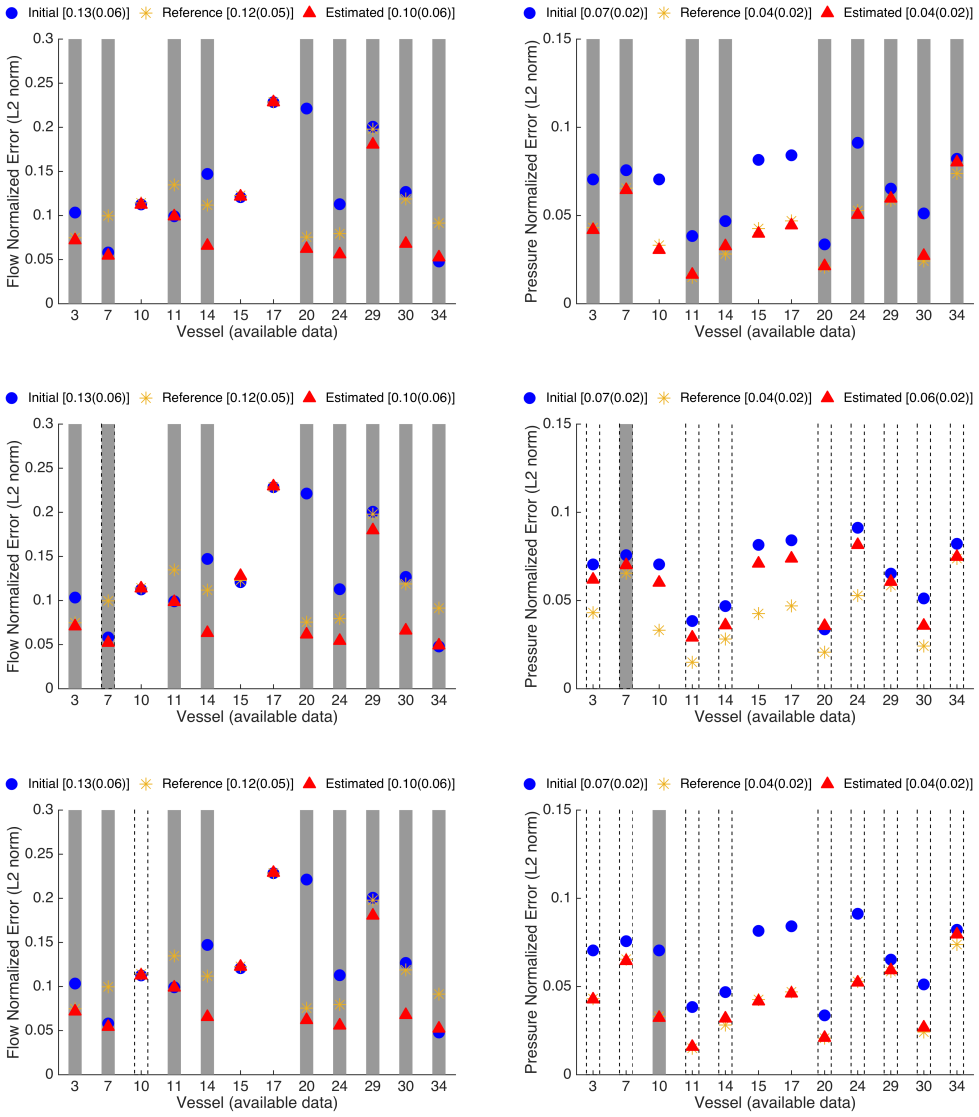

Figure 9: Summary of the errors obtained running the one-dimensional model with the initial values of the resistances (blue), with the reference values (yellow) and with the estimated parameters (red), in the case of using all flow data and pressure data at all flow measurement locations (top row), at the right ulnar artery (vessel 7, middle row) and at the aortic arch (vessel 10, bottom row). The x-axis indicates the observed vessel, while the y-axis shows the corresponding error. Errors average (standard deviation) are shown for each model setting in the legends. Left: errors with respect to flow data. Right: errors with respect to pressure data. Grey bars denote vessels for which measurements of the quantity for which the error is computed have been used in the estimation, whereas dashed lines indicate vessels for which a measurement of the other quantity has been used for the estimation. For example, a vessel with dashed lines in the pressure error plot indicates that the flow measurement in this vessel was used for the estimation, and viceversa.

3.2 Estimation of one terminal bifurcation

The previous benchmark evidenced the higher sensitivity of flow measurement to terminal resistances, with respect to pressure measurements. The goal of the following test is to investigate more in detail how the accuracy of the estimate of terminal parameters depends on flow measurements on the corresponding branches (the most sensitive and favorable scenario). We focus on the terminal branch defined by the right anterior and right posterior tibial arteries (vessels 34 and 35 in Figure 1). Among the available measured flows, we select the flow rate in the right iliac-femoral artery III (vessel 30) and in the right posterior tibial artery (vessels 34). Notice that, in previous studies concerning the ROUKF for estimation of terminal resistances [32, 3, 18], the flow measurements in the corresponding branch were used. However, in our case the data in the right anterior artery were not available. On the other hand, since the two considered terminal branches are originated from the right iliac-femoral artery III (vessel 30), the measurements in vessels 30 and 34 allow to characterize the flow through both terminals 34 and 35.

For this test, we generate a set of initial conditions, parameterizing the resistances as $R_i = 2^{\theta_i}$ ($i = 34, 35$) and taking equally spaced values of θ_{34} and θ_{35} in the interval $[-2, 2]$. For each different initial guess pair (R_{34}, R_{35}), we first generate an initial state running the corresponding forward model until reaching a periodic regime. Next, we apply the Kalman filter, using either synthetic measurements or experimental observations. In all considered cases, the filter converged in about 150 cycles (around 120 s, corresponding to few minutes of wall clock time).

Using synthetic measurements, both parameters rapidly approach the exact values (Figure 10, left), almost independently from the initial guess, yielding estimates $R_{34} = 5.13 \pm 0.12$ and $R_{35} = 5.61 \pm 0.21$ (i.e. errors below 1% with respect to the reference parameter). Employing

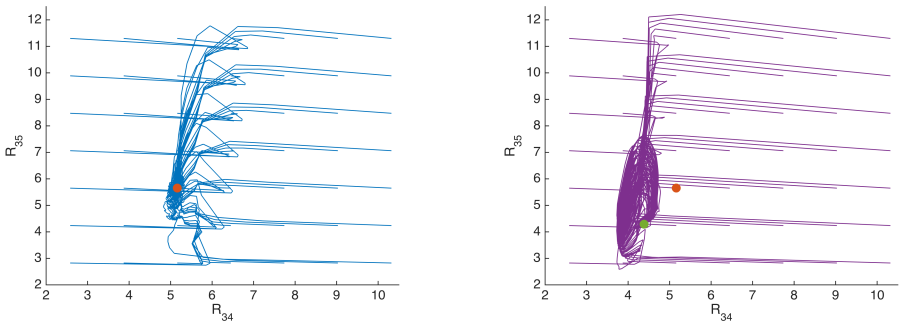

Figure 10: Estimated terminal resistance R_{34} and R_{35} using flow measurements in vessels 30 and 34. The plot shows the trajectory of the solution in the space (R_{34}, R_{35}) over time (running the Kalman filter), depending on the different initial guesses (x- and y-axes). In each plot, the red circle indicates the reference solution, while the green circle (right plot) shows the average of the estimated values using experimental measurements. Left: results with synthetic flow measurements (mean values 5.15 and 5.67, respectively – superimposed to the reference ones). Right: results with experimental flow measurements (mean values 4.39 and 4.29, respectively).

experimental measurements (Figure 10, right), we obtained mean estimated parameters $R_{34} =$

4.68 and $R_{35} = 4.53$ (differences of 15% and 24% respect to reference values, respectively).

Running the forward one-dimensional model using the estimated resistances obtained from the experimental flow measurements, one obtains a slight improvement in the error for the measured vessels (Figure 11, left), while the errors with respect of the remaining flow data are comparable with the discrepancies obtained with reference parameters. On the other hand, errors with respect to pressure measurements slightly increase (Figure 11, right).

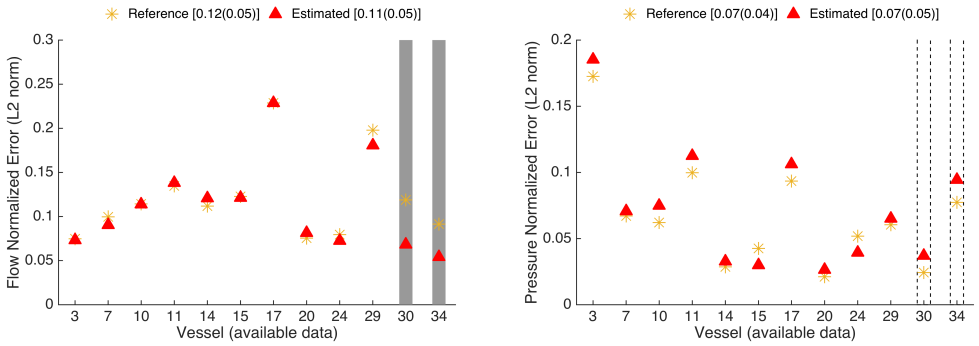

Figure 11: Summary of the errors obtained running the one-dimensional model with the reference values of the resistances of terminal vessels 34 and 35 (yellow) and with the mean of estimated parameters (red), in the case of using flow data on vessel 30 and 34. The x-axis indicates the observed vessel, while the y-axis shows the corresponding error. Errors average (standard deviation) are shown for each model setting in the legends. Left: errors with respect to flow data. Right: errors with respect to pressure data. Grey bars denote vessels for which measurements of the quantity for which the error is computed have been used in the estimation, whereas dashed lines indicate vessels for which a measurement of the other quantity has been used for the estimation. For example, a vessel with dashed lines in the pressure error plot indicates that the flow measurement in this vessel was used for the estimation.

Moreover, we also notice (not shown) that a relevant improvement is obtained for the mean flow rates, for which the errors become extremely low (below 1%) using the parameters estimated by the filter (with respect to original errors of 12% and 7% for the reference parameters). This result is consistent with the fact that the major effect of a terminal resistance is seen in the mean flow rate of the corresponding terminal branch, rather than in the flow profile over time.

	R_{34}	R_{35}	$e^{Q_{30}}$	$e^{Q_{30}^{\text{mean}}}$	$e^{Q_{34}}$	$e^{Q_{34}^{\text{mean}}}$
Reference values	5.16	5.65	20.3	12.4	10.2	7.4
Estimated values – Mean (RMS)	4.68 (0.06)	4.53 (0.08)	11.8	0.7	7	0.04

Table 2: Summary of results for the estimated terminal resistances R_{34} and R_{35} (in mmHg ml s^{-1}) and corresponding relative errors (%), using experimental measurements of flow in vessels 30 and 34.

We now address the estimation of terminals 34 an 35 using a single experimental flow measurement in vessel 30 (i.e., before the terminal bifurcation). The results (see Figure 12) demonstrate that the filter is not able to correctly identify both parameters, and very differ-

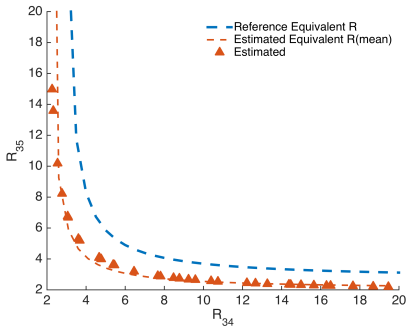

Figure 12: Estimated terminal resistances for different initial guesses (final values, red triangles), compared with the curve $\left(\frac{1}{R_{34}}+\frac{1}{R_{35}}\right)^{-1}=2.70$ (dashed blue line) defining the reference equivalent resistance and with the curve $\left(\frac{1}{R_{34}}+\frac{1}{R_{35}}\right)^{-1}=2.03$ (dashed red line).

ent estimations are obtained for different initial guesses. However, the values of the estimated terminal resistances are such that the equivalent resistance lies close to the manifold defined by the equivalent reference resistance of the two terminal branches

$$\left(\frac{1}{R_{34}}+\frac{1}{R_{35}}\right)^{-1}=R^{eq}_{34,35}=2.70\ \text{mmHg ml s}^{-1}\,.$$

More in detail, the average estimated value of the equivalent resistance is 2.03 mmHg ml s^{-1}.

3.3 Discussion

In conclusion, concerning the estimation of terminal resistances, our results suggest that flow measures (close to the terminal vessels) have in general higher sensitivity than pressure measurements. However, pressure measures result more correlated with each other, yielding more stable estimations (although less accurate) considering the whole parameter set. The combination of flow measurements and at least one pressure measurement has shown to be mandatory in order to obtain consistent parameter estimates in simultaneous relation to both flow rate and pressure. Moreover, the results obtained here indicate that the pressure estimation is more accurate when the single pressure measurement is acquired at a central location, Comparing the results of the in silico and the in vitro estimations, the main outcome is that employing in vitro measurements in general makes the identification problem more visible, while, using synthetic measurements might yield satisfactory estimates also for the less identifiable parameters. This last observation, even if rather obvious, should be taken into account by practitioners that try to estimate parameters in more complex settings.

Finally, it is worth commenting on the sensitivity of the results with respect to the filter parameters σ^2_{param} and σ^2_{obs} (parameters and measure covariances). Our numerical study (not reported here) showed that increasing the covariances tends to improve the estimates for the more identifiable parameters, reducing at the same time the convergence time. In contrast, for the parameters to which the measures are less sensitive, larger covariances produce unstable

estimates (diverging in time), which eventually might lead to numerical instability in the forward solver.

4 Estimation of arterial wall properties

The estimation of arterial wall properties strongly depends on modeling choices, i.e., on the particular choice of tube law (2). For the one dimensional model of the in vitro arterial network under consideration [1], the tube law has the form

$$p = \frac{\beta}{A_0}(\sqrt{A} - \sqrt{A_0}) + \frac{\Gamma}{a_0\sqrt{A}}\frac{\partial A}{\partial t}, \tag{20}$$

with

$$\beta = \frac{4}{3}\sqrt{\pi}Eh, \quad \Gamma = \frac{2}{3}\sqrt{\pi}\Phi h, \tag{21}$$

where Φ is the viscosity of silicone, E is the vessel Young's modulus, h is the vessel wall thickness and A_0 is the reference cross-sectional area of the vessel.

From a clinical point of view, we are interested in estimating the vessel stiffness, which can be a relevant indicator in case of cardiovascular pathologies. For tube law (20) the stiffness is mainly determined by the Young's modulus (E) and the wall thickness (h). Moreover, since (20) is linear in hE, from the point of view of the estimation it will be equivalent to consider either h, or E, or the product hE as unknown parameter. In fact, any variation in one of these parameters will have – up to a multiplicative factor – the same impact on model predictions. However, for the considered problem, the substantial difference between h and E is that all vessels have the same Young's modulus $E_0 = 1.2$ MPa, while thicknesses vary along the network.

Remark 2. *In particular, also the sensitivities of the model with respect to h or E (and hence the corresponding GSFs) are equal up to a multiplicative factor.*

4.1 Wall thickness along the aorta

First, in order to test the robustness of the filter, we consider the estimation of wall thicknesses in the eight aortic segments. We consider the following relationship between thickness and vessel radius [5] to define the initial guesses

$$h(R_0) = R_0\left(a\mathrm{e}^{bR_0} + c\mathrm{e}^{dR_0}\right), \tag{22}$$

with $a = 0.2802$, $b = -5.053$ cm^{-1}, $c = 0.1324$, $d = -0.1114$ cm^{-1} and $R_0 = \sqrt{A_0/\pi}$.

The initial values of thickness are summarized in Table 3, together with the reference values [1]. Observe that these initial values are, in all cases, about three times larger than the reference ones. For the estimation, we consider the available measurements in three segments of the aorta (vessels 10, 15 and 17 in Figure 1, right), two measurements in the abdominal region (splenic and left renal arteries, vessels 20 and 24, respectively), two peripheral measurements in the upper part of the body (left subclavian and right carotid arteries, vessel 3 and 11, respectively) and a peripheral measurement in the upper part of the body (right iliac femoral

Vessel	1	8	10	15	17	23	25	27
Initial [cm]	1.56	1.47	1.41	1.34	1.22	1.07	1.00	0.90
Reference [cm]	0.51	0.5	0.41	0.43	0.34	0.33	0.35	0.3
$\frac{\text{Initial}}{\text{Reference}}$	3.1	2.9	3.4	3.1	3.6	3.2	2.9	3.0

Table 3: The wall thicknesses obtained from (22) (second row) compared to the reference values of [1] (third row).

artery, vessel 30). Concerning the filter parameters, we choose $\gamma = 10^2$ and $\sigma^2_{\text{param}} = 0.1$. Moreover, we observe an important impact of the sampling period Δt_F on the convergence of the estimation procedure. In practice, Δt_F had to be sufficiently large to allow the information of parameter correction to reach the measurement locations. The results shown in this section have been obtained using $\Delta t_F = 0.1$ s and running the filter algorithm up to a time of 500 s (about 600 cardiac cycles), yielding a computational time of about 40 minutes.

4.1.1 Estimation using flow measurements

We begin the study analyzing the Fischer information matrix and the generalized sensitivity function of the set of parameters with respect to the selected set of observations. Considering flow measurements, the Fischer information matrix (Figure 13, left) shows that 4 segments (1, 15, 17 and 27) have the least correlation with the others. This result is in accordance with the fact that, one the one hand, the sensitivity of the measurements with respect to the thickness of vessels 15 and 17 shall be higher (as these vessels are also under observation), while vessel 27 might be more important for the flow measured downstream. Concerning vessel 1, notice that this is the first segment of the network, in which the (flow) boundary condition is imposed. On the other hand, the segment 25 appears to be the less identifiable. Indeed,

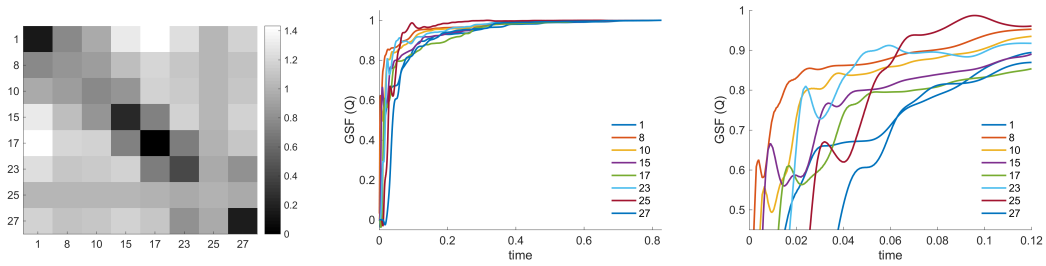

Figure 13: Identifiability study for the thickness (h) of aorta segments (vessels 1, 8, 10, 15, 17, 23, 25, 27) using flow observations in vessels 3, 10, 11, 15, 17, 20, 24 and 30). Left: Fischer information matrix. Center: GSF over a period. Right: zoom of the GSF profiles in the interval $[0, 0.1]$s.

notice that vessel 25 is quite short, with a length of $0.7\,cm$, which reduces its contribution to the sensitivity matrix. The profiles of the GSFs (Figure 13, center) reveal that the information contained in the selected measurements is concentrated at the very beginning of the cycle (before 0.4 seconds). This can reflect the fact that the system quickly perceives the change in the thickness because the aorta is a central artery, close to all other vessels, and then no

further information can be gained when time runs. All vessels have very similar GSF profiles. However, considering closely the different profiles (Figure 13, right) one notices that the segments 8, 10, 15 and 25 have a slightly more oscillating behavior, which could indicate potential identifiability problems.

The final estimates are depicted in Figure 14. Using synthetic measurements, the vessels 1, 15, 17 and 27 are close to reference values (consistently with the prediction of the identifiability analysis), while, concerning the remaining parameters, we observe considerable improvements for vessels 8, 10 and 23 (for which the difference from the reference thickness is almost halved). On the other hand, the filter is not able to properly modify the thickness of vessel 25, as the sensitivity of the measurements with respect to this parameter is very low (Figure 13). In the in vitro case, the estimates are generally not that close to the reference values, but one can clearly appreciate an overall improvement in the final estimated parameters, as the differences with respect to the reference values are almost halved. The only exception is, as before, vessel 25, which is hardly modified by the filter.

Hence, one can conclude that the combination of Fischer information matrix and GSF is once more a useful indicator about the potential of the filter and on the feasibility of parameter identification (specifically concerning the identifiability of vessel 25).

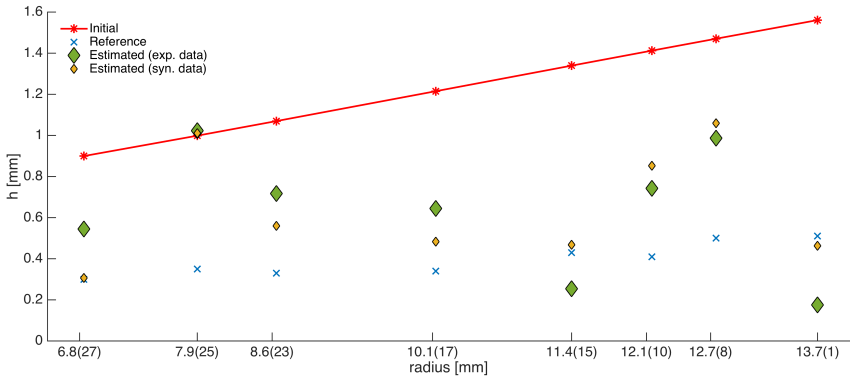

Figure 14: Estimated wall thicknesses using flow measurements (synthetic and experimental). In all cases, the estimated thickness is compared with initial guesses (red line) and reference values (crosses).

The fact that the estimated values are not precisely the reference ones deserves further analysis. When considering synthetic measurements, the discrepancy can be explained by the fact that estimating 8 parameters at the same time yields a sigma-points stencil relatively far from the initial condition. This aspect, combined with the non-linearity present in the model, might prevent the filter from reaching the target solution. Concerning the in vitro case, one can also consider the errors between the considered experimental measurements and the numerical solution corresponding to the new parameters, compared to the discrepancies obtained using the reference values [1]. These results are summarized in Figure 15, showing that estimated parameters considerably reduce errors, performing even better than the reference values. Another conclusion that can be extracted from this figure is that the estimation of wall thickness using flow data does not deteriorate the pressure values predicted by the model. Hence, even if the values of the thickness differ from the reference ones, the error analysis reveals that the filter might modify these parameters to improve a potential modeling deficiency. In fact, in the

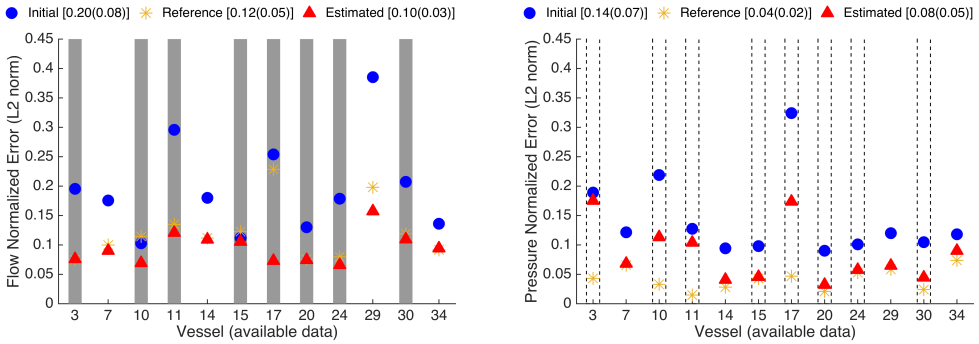

Figure 15: Summary of the errors obtained running the one-dimensional model with the initial values of resistances (blue), with the reference values (yellow) and with the estimated parameters (red), in the case of flow data. The x-axis indicates the observed vessel, while the y-axis shows the corresponding error. Errors average (standard deviation) are shown for each model setting in the legends. Left: errors with respect to flow data. Right: errors with respect to pressure data. Grey bars denote vessels for which measurements of the quantity for which the error is computed have been used in the estimation, whereas dashed lines indicate vessels for which a measurement of the other quantity has been used for the estimation. For example, a vessel with dashed lines in the pressure error plot indicates that the flow measurement in this vessel was used for the estimation.

case of experimental measurements, the estimation of the parameters also depends on how close the mathematical model is to the *real* experiment.

4.1.2 Estimation using pressure measurements

The situation is slightly different considering pressure measurements. From the Fischer information matrix (Figure 16, left) one can conclude that, while vessel 17 (which is also measured) has very low correlations with the remaining ones (the vessel 17 is also observed), vessels 8 and 25 might suffer from identifiability problems. The profiles of the GSFs (Figure 16, right) show that vessels 10 and 17 (both corresponding to measured vessels) are expected to be the more identifiable, while the estimation of vessels 25 and 27, which have the most oscillatory profiles (in particular, vessel 25 is the only one with GSF overshooting the interval [0,1]), could result more difficult. The remaining GSFs are rather complex, showing small amplitude oscillations up to time 0.4 s (as for the case of flow measurements), combined with an overall monotone increasing behavior.

Also in this case, the theoretical expectations are reflected into the final estimates (Figure 17). In the in silico case, a good agreement with reference parameters is obtained for vessels 1, 10, 15 and 17, while the estimates for vessels 8 and 25, which showed the higher correlations with the rest of parameters, remain close to the initial value (hence about three times larger than the reference thickness). The result is worse for vessel 27 (characterized by an oscillating GSF) and vessel 23, which could suffer from the worse estimates in the downstream segments 25 and 27. However, in these two cases the difference with respect to the reference values is drastically reduced. The in vitro estimation appears even more consistent with the

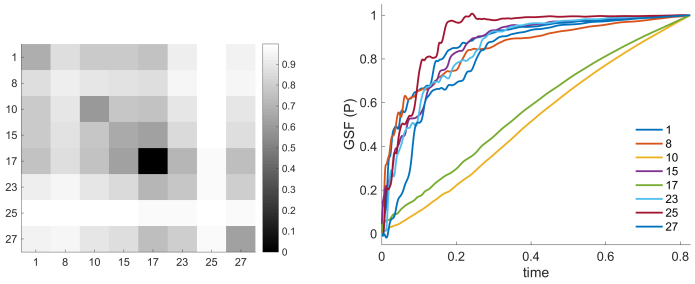

Figure 16: Identifiability study for the aorta thickness (h) (vessels 1, 8, 10, 15, 17, 23, 25, 27) using pressure observations in vessels 3, 10, 11, 15, 17, 20, 24 and 30). Left: Fischer information matrix. Right: GSF over a period.

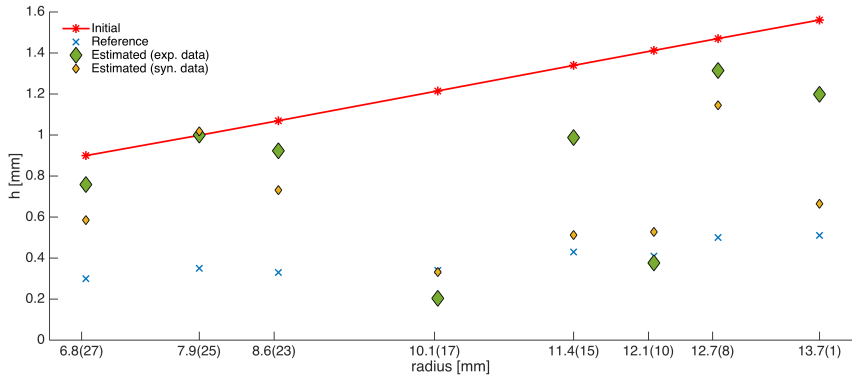

Figure 17: Estimated wall thickness using pressure measurements (synthetic and experimental). In all cases, the estimated values of thicknesses are compared with initial guesses (red line) and reference values (crosses).

expectations of the identifiability analysis. In particular, vessels 10 and 17, the only segments characterized by a monotone GSF, reach parameter values close to the reference ones, while the remaining thicknesses decrease (except for vessel 25). Nevertheless, in general, the values remain closer to the initial guesses than in the case of flow measurements. Note that, in the in silico case, also the intermediate vessel 15 (oscillatory GSF) is well estimated, while this does not happen in the in vitro test. As a conclusion, the results of Figures 16–17 reveal that the estimation of arterial wall parameters using pressure data might be, in general, complicated, and that the quality of the estimation is extremely sensitive to the location of the measurements.

Finally, in Figure 18 we monitor the errors between the experimental measurements and the numerical solution obtained using the new parameters or the reference ones. For all measured vessels, both estimated and reference parameters achieve very similar errors (mainly below 0.1), and vessel 17 is the one showing the highest difference (error of 0.1 with the reference parameters, lowered to about 0.08 with the new set). This confirms the above statement that pressure data might be less sensitive than flow data to wall parameter changes. Moreover, the reduction of errors for flow rate with respect to the ones obtained using initial guesses of

parameters are satisfactory, as when flow measurements where used for the estimation.

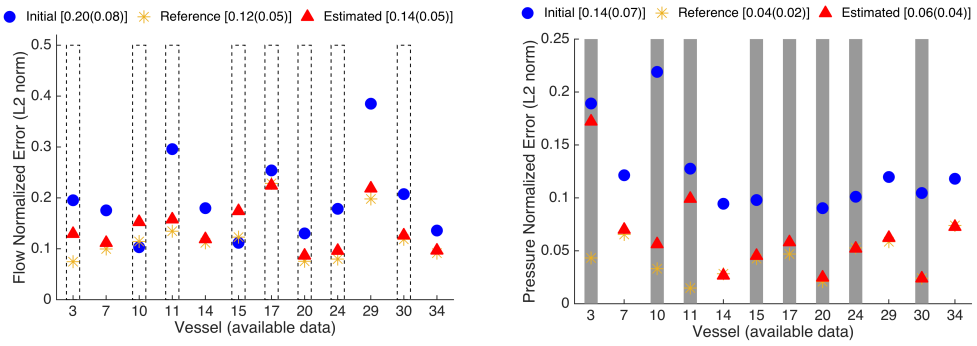

Figure 18: Summary of the errors obtained running the one-dimensional model with the initial values of wall thickness (blue), with the reference values (yellow) and with the estimated parameters (red), in the case of pressure data. The x-axis indicates the observed vessel, while the y-axis shows the corresponding error. Errors average (standard deviation) are shown for each model setting in the legends. Left: errors with respect to flow data. Right: errors with respect to pressure data. Grey bars denote vessels for which measurements of the quantity for which the error is computed have been used in the estimation, whereas dashed lines indicate vessels for which a measurement of the other quantity has been used for the estimation. For example, a vessel with dashed lines in the pressure error plot indicates that the flow measurement in this vessel was used for the estimation. Notice that the data point of the error for initial guess of vessel 17 (pressure), is outside the plot range.

Since errors of forward simulations performed using the estimated parameters obtained with flow or pressure measurement are similar, we do not expect any benefit from combining pressure and flow measurements in terms of error reduction. In fact, running tests similar to those presented in Section 3, confirmed this statement (results not shown here).

4.2 Aorta stiffness

As next, we consider the estimation of the Young's modulus of the aorta, considering a *single* parameter for vessel segments 1,8, 10, 15, 17, 23, 25 and 27. The reference value (the same for all vessels also in the experimental setup) is $E = 1.2$ MPa.

The aim of this test is to assess the accuracy of the filter, also depending on the particular initial guess. To this purpose we consider several initial values for the parameter, regularly spaced between 0.6MPa (50% of error) and 2.4 MPa (100% of error). For each initial guess of the Young's modulus, we run the forward one-dimensional model until a periodic regime is reached, in order to generate a consistent initial state in the whole network. Next, we run the Kalman filter up to 500 s, corresponding to about 600 cardiac cycles.

For the estimation, we consider the measurements in two segments of the aorta (vessels 10 and 17 in Figure 1, right), a peripheral measurement in the upper part of the body (left subclavian artery – vessel 3) and a peripheral measurement in the lower part of the body (right iliac femoral artery, vessel 30). The filter parameters are chosen as $\sigma^2_{\text{param}} = 0.4$, $\gamma = 10^4$,

$\Delta t_F = 0.1$ s.

The results of the estimation algorithm are displayed in Figure 19, showing the values of the parameters over time. In particular, using synthetic data, the filter always delivers very accurate results, both in the case of flow and pressure measurements. The only exception is the initial condition $E = 0.6$ MPa, for which the filter converges to a slightly lower value.

This effect is more pronounced using pressure measurements (for which the parameter initialized with 0.6MPa converges to 1 MPa). Moreover, flow measurements yield a faster filter convergence. These facts confirm that pressure data might be less sensitive to mechanical properties and that they are more affected by non-linear effects. In the case of experimental measurements one can draw similar conclusions. However, the estimated Young's moduli are slightly lower (on average, 0.98 MPa for flow measurements and 1.03 MPa for pressure measurements). The final results are independent from the initial conditions, with the exception of the initial Young's modulus of 0.6 MPa, yielding slightly lower estimates.

Finally, Figure 20 serves to verify that running the forward one dimensional model with the provided estimates for the in vitro case, although lowering the Young's modulus by about 16%, results in slightly smaller errors (than the reference parameters) with respect to the considered measurements. As previously stated, this indicates that the filter tends to estimate the parameters in order to compensate for modeling deficiencies.

4.3 Discussion

The estimation of arterial wall properties turned out to be a more difficult task for the filter than the estimation of terminal resistances, in terms of convergence time. Also in this case we observed that flow measurements allow in general a more robust estimation, while pressure data yields a scenario which is less sensitive to parameter changes.

At the same time, it can be noticed that, especially for the study of mechanical properties, the identifiability analysis based on combining Fischer information matrix and GSFs resulted in an accurate tool to distinguish more robustly identifiable parameters as well predicting potential problems in the in vitro estimation.

Concerning the sensitivity of the results with respect to the filter parameters σ^2_{param} and σ^2_{obs} (parameters and measure covariances), we obtained similar results as in the case of terminal resistances. Namely, larger covariances tend to affect more (in a negative way) the estimation of less identifiable parameters, especially in the in vitro case.

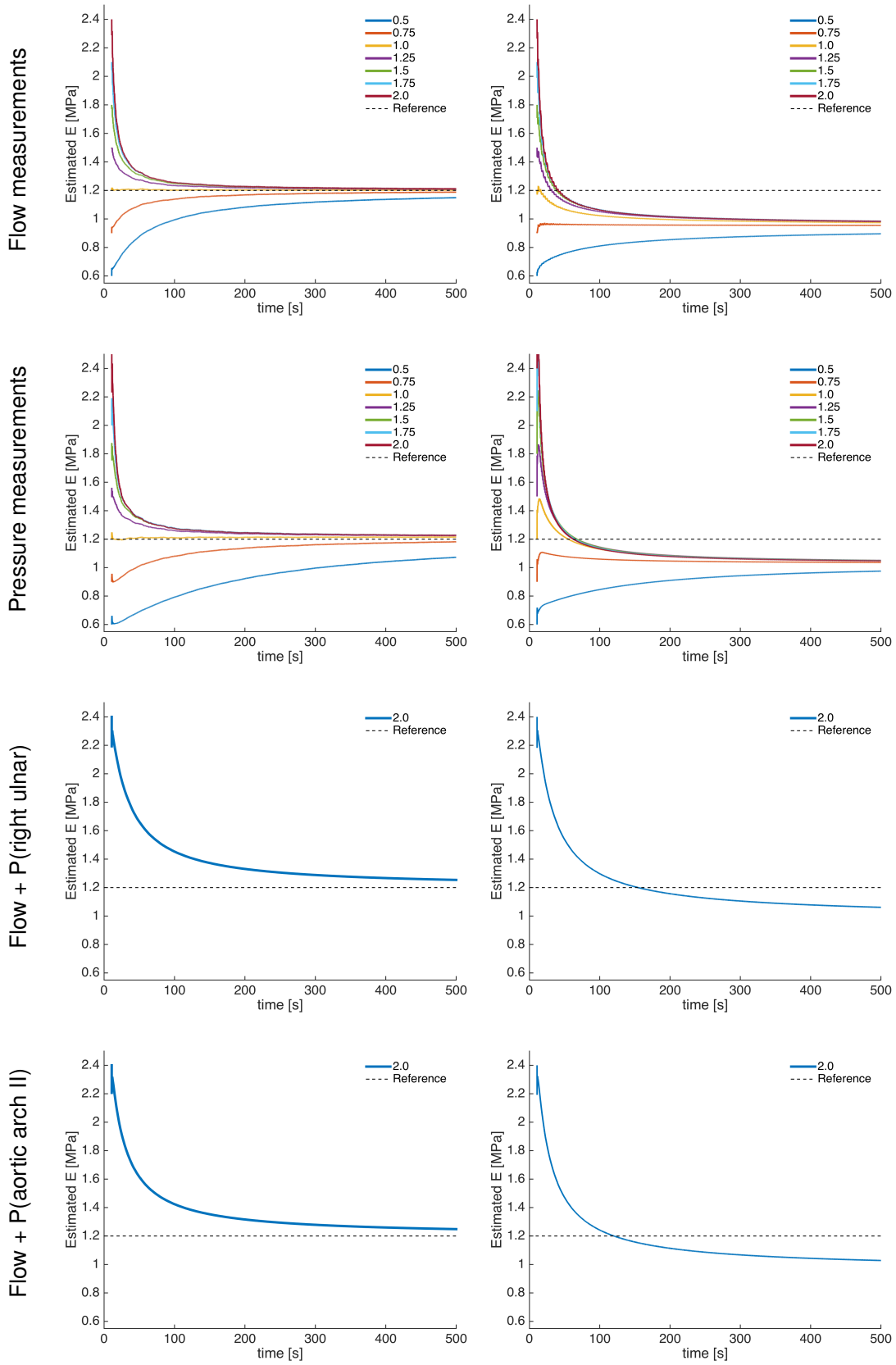

Figure 19: Estimated Young's modulus in the aorta, using flow (top) or pressure (bottom) observations. Left: results with synthetic measurements (perturbed with 5% of noise). Right: results with experimental measurements.

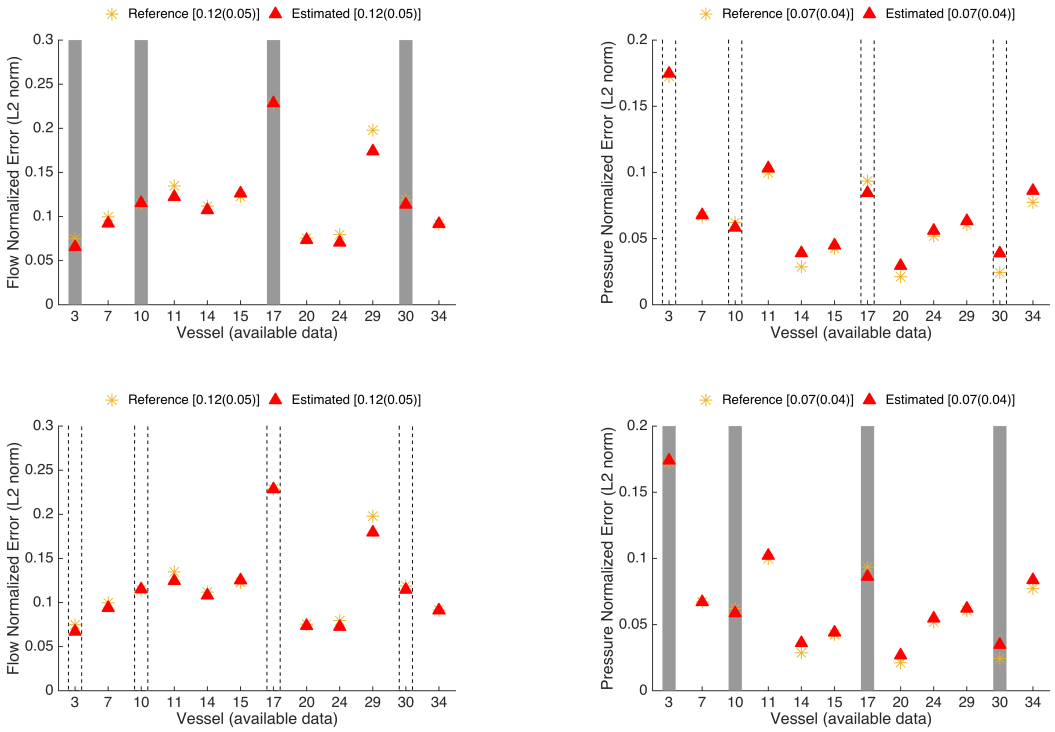

Figure 20: Summary of the errors obtained running the one-dimensional model with the reference and with the estimated Young's moduli, The x-axis indicates the observed vessel, while the y-axis shows the corresponding error, obtained using the average value estimated by the Kalman filter with different initial conditions. Errors average (standard deviation) are shown for each model setting in the legends. Left: flow data, using $E = 0.98$ MPa for the forward simulation. Right: pressure data, using $E = 1.03$ MPa for the forward simulation. The reference errors are obtained with $E = 1.2$ MPa [1].

5 Conclusion

We assessed the performance of the reduced order unscented Kalman filter applied to a one-dimensional blood flow model in a realistic, though controlled, setting, by considering an in vitro experiment [1] for which a set of flow and pressure measurements is available.

In particular, we considered (i) the estimation of the resistances of terminal vessels (used for boundary conditions) and (ii) the estimation of arterial wall properties related to vessel mechanics (thickness and Young's modulus). In both cases, we investigated the robustness of the filter, by considering the joint estimation of several parameters, and its accuracy, focusing on one or two parameters, but considering several initial conditions. Moreover, prior to the estimation tests, we performed a detailed identifiability analysis based on the Fischer information matrix (to quantify the covariances between the parameters) and on the generalized sensitivity function (to assess the quantity of information contained in the measurements). For each considered test, we compared the estimates obtained with in silico data (i.e., numerical results perturbed with Gaussian noise) and in vitro measurements [1]. At the same time, we considered both flow-driven and/or pressure-driven estimations.

The first outcome of our study is that the estimation based on in silico data resulted, in all cases, more stable than the one based on in vitro data. In particular, some parameters featuring a low identifiability (low sensitivity and/or high covariance) could be estimated in the in synthetic (in silico) setup, but not in the experimental (in vitro) one. In the context of parameter identifiability, our results also show that a detailed identifiability analysis provides useful information about the performance of the filter (especially when considering in vitro data). A further aspect, which distinguished in silico from in vitro estimation, is the time needed by the filter to reach convergence, which in the latter case resulted always longer.

Considering the difference of using flow or pressure measurements to feed the Kalman filter, the numerical tests revealed that flow data have a higher sensitivity with respect to terminal resistances, especially close to the vessel, hence yielding precise estimates in those cases. However, the estimates might deteriorate if the observations are acquired far from the terminal locations. Moreover, it should be noted that the use of combinations of flow and (some or even a single) pressure measurements yielded better results for the estimation of terminal resistances, when comparing the model outcomes in terms of flow rate and pressure values. In the case of arterial wall properties, flow measurements seem to contain a larger amount of information about the parameters. In fact, considering pressure data, only the parameters located on (or close to) observed vessels could be accurately estimated. These conclusions are in agreement with the fact that the pressure pulse is formed from the interaction of many forward and backward running waves, and its characterization depends upon global and distributed features of the circulatory system. In turn, flow waveforms features are related to local characteristics of the arterial network.

A final comment on the filter estimates is in order. The parameters may appear inaccurately estimated when compared with reference values. Nevertheless, it is important to recall that the error with respect to the measurements given by the estimated parameters is always smaller than the one obtained with reference values. This highlights the presence of modeling errors between the experimental setting and the model used in the simulations. In other words, the reference parameters may have no direct relation with the optimal solution obtained by the filter, because the filter is capable of compensating deficiencies of the model by choosing parameters so that errors with respect to experimental measurements are further reduced.

References

[1] Alastruey, J., Khir, A.W., Matthys, K.S., Segers, P., Sherwin, S.J.: Pulse wave propagation in a model human arterial network: Assessment of 1-D visco-elastic simulations against *in vitro* measurements. Journal of Biomechanics **44**, 2250–2258 (2011)

[2] Alastruey, J., Parker, K.H., Peiró, J., Byrd, S.M., Sherwin, S.J.: Modelling the circle of Willis to assess the effects of anatomical variations and occlusions on cerebral flows. Journal of Biomechanics **40**, 1794–1805 (2007)

[3] Bertoglio, C., Moireau, P., Gerbeau, J.F.: Sequential parameter estimation for fluid-structure problems. application to hemodynamics. Int. J. Numer. Meth. Biomed. Eng. **28**, 434–455 (2012)

[4] Bessems, D., Giannopapa, C.G., Rutten, M.C., van de Vosse, F.N.: Experimental validation of a time-domain-based wave propagation model of blood flow in viscoelastic vessels. Journal of Biomechanics **41**(2), 284 – 291 (2008). DOI http://dx.doi.org/10.1016/j.jbiomech.2007.09.014. URL http://www.sciencedirect.com/science/article/pii/S0021929007003922

[5] Blanco, P.J., Watanabe, S.M., Dari, E.A., Passos, M.R.F., Feijóo, R.A.: Blood flow distribution in an anatomically detailed arterial network model: criteria and algorithms. Biomech. Model Mechanobiol. **13**(6), 1303–1330 (2014)

[6] Blanco, P.J., Watanabe, S.M., Passos, M.R.F., Lemos, P.A., Feijóo, R.A.: An anatomically detailed arterial network model for one-dimensional computational hemodynamics. IEEE Transactions on Biomedical Engineering **62**(2), 736–753 (2015). DOI 10.1109/TBME.2014.2364522

[7] Boileau, E., Nithiarasu, P., Blanco, P.J., Müller, L.O., Fossan, F.E., Hellevik, L.R., Donders, W.P., Huberts, W., Willemet, M., Alastruey, J.: A benchmark study of numerical schemes for one-dimensional arterial blood flow modelling. International Journal for Numerical Methods in Biomedical Engineering pp. n/a–n/a (2015). DOI 10.1002/cnm.2732. URL http://dx.doi.org/10.1002/cnm.2732

[8] DeVault, K., Gremaud, P.A., Novak, V., Olufsen, M.S., VerniÃÍres, G., Zhao, P.: Blood flow in the circle of willis: Modeling and calibration. Multiscale Modeling & Simulation **7**(2), 888–909 (2008). DOI 10.1137/07070231X

[9] Dumbser, M., Enaux, C., Toro, E.F.: Finite volume schemes of very high order of accuracy for stiff hyperbolic balance laws. Journal of Computational Physics **227**, 3971–4001 (2008)

[10] Dumbser, M., Toro, E.F.: A Simple Extension of the Osher Riemann Solver to Non-conservative Hyperbolic Systems. Journal of Scientific Computing **48**, 70–88 (2011)

[11] Formaggia, L., Lamponi, D., Quarteroni, A.: One-dimensional models for blood flow in arteries. Journal of Engineering Mathematics **47**, 251–276 (2003)

[12] Formaggia, L., Quarteroni, A., Veneziani, A.: Cardiovascular Mathematics: Modeling and simulation of the circulatory system. Springer-Verlag Italia, Milano (2009)

[13] Huberts, W., Bode, A., Kroon, W., Planken, R., Tordoir, J., van de Vosse, F., Bosboom, E.: A pulse wave propagation model to support decision-making in vascular access planning in the clinic. Medical Engineering & Physics **34**(2), 233 – 248 (2012). DOI http://dx.doi.org/10.1016/j.medengphy.2011.07.015. URL http://www.sciencedirect.com/science/article/pii/S1350453311001809

[14] Huberts, W., Canneyt, K.V., Segers, P., Eloot, S., Tordoir, J., Verdonck, P., van de Vosse, F., Bosboom, E.: Experimental validation of a pulse wave propagation model for predicting hemodynamics after vascular access surgery. Journal of Biomechanics **45**(9), 1684 – 1691 (2012). DOI http://dx.doi.org/10.1016/j.jbiomech.2012.03.028. URL http://www.sciencedirect.com/science/article/pii/S0021929012001947

[15] Julier, S.: The spherical simplex unscented transformation. In: Proc. of the American Control Conference, pp. 2430–4234 (2003)

[16] Liang, F.Y., Fukasaku, K., Liu, H., Takagi, S.: A computational model study of the influence of the anatomy of the circle of willis on cerebral hyperperfusion following carotid artery surgery. BioMedical Engineering OnLine **10**(1), 84 (2011). DOI 10.1186/1475-925X-10-84. URL http://www.biomedical-engineering-online.com/content/10/1/84

[17] Liang, F.Y., Takagi, S., Himeno, R., Liu, H.: Biomechanical characterization of ventricular-arterial coupling during aging: A multi-scale model study. Journal of Biomechanics **42**, 692–704 (2009)

[18] Lombardi, D.: Inverse problems in 1D hemodynamics on systemic networks: a sequential approach. Int. J. Numer. Method Biomed. Eng. **30**(2), 160–179 (2014)

[19] Matthys, K.S., Alastruey, J., Peiró, J., Khir, A.W., Segers, P., Verdonck, P.R., Parker, K.H., Sherwin, S.J.: Pulse wave propagation in a model human arterial network: Assessment of 1-D numerical simulations against *in vitro* measurements. Journal of Biomechanics **40**, 3476–3486 (2007)

[20] Moireau, P., Chapelle, D.: Reduced-order Unscented Kalman Filtering with application to parameter identification in large-dimensional systems. Esaim Contr. Opt. Calc. Var. **17**, 380–405 (2011)

[21] Montecinos, G., Müller, L., Toro, E.F.: Hyperbolic reformulation of a 1D viscoelastic blood flow model and ADER finite volume schemes. Journal of Computational Physics **266**, 101–123 (2014). DOI 10.1016/j.jcp.2014.02.013

[22] Montecinos, G.I., Castro, C.E., Dumbser, M., Toro, E.F.: Comparison of solvers for the generalized riemann problem for hyperbolic systems with source terms. Journal of Computational Physics **231**, 6472–6494 (2012)

[23] Müller, L., Toro, E., Haacke, E., Utriainen, D.: Impact of ccsvi on cerebral haemodynamics: a mathematical study using mri angiographic and flow data. Phlebology (2015). DOI 10.1177/0268355515586526. URL http://phl.sagepub.com/content/early/2015/06/01/0268355515586526.abstract

[24] Müller, L.O., Blanco, P.J.: A high order approximation of hyperbolic conservation laws in networks: Application to one-dimensional blood flow. Journal of Computational Physics

300, 423 – 437 (2015). DOI http://dx.doi.org/10.1016/j.jcp.2015.07.056. URL http://www.sciencedirect.com/science/article/pii/S0021999115005094

[25] Müller, L.O., Blanco, P.J., Watanabe, S.M., Feijóo, R.: A high-order local time stepping finite volume solver for one-dimensional blood flow simulations: application to the adan model. International Journal for Numerical Methods in Biomedical Engineering pp. n/a–n/a (2016). DOI 10.1002/cnm.2761. URL http://dx.doi.org/10.1002/cnm.2761

[26] Müller, L.O., Leugering, G., Blanco, P.J.: Consistent treatment of viscoelastic effects at junctions in one-dimensional blood flow models. Journal of Computational Physics **314**, 167–193 (2016)

[27] Müller, L.O., Toro, E.F.: Well-balanced high-order solver for blood flow in networks of vessels with variable properties. International Journal for Numerical Methods in Biomedical Engineering **29**(12), 1388–1411 (2013)

[28] Müller, L.O., Toro, E.F.: A global multiscale mathematical model for the human circulation with emphasis on the venous system. International Journal for Numerical Methods in Biomedical Engineering **30**, 681–725 (2014). DOI 10.1002/cnm.2622

[29] Mynard, J.P., Davidson, M.R., Penny, D.J., Smolich, J.J.: A simple, versatile valve model for use in lumped parameter and one-dimensional cardiovascular models. International Journal for Numerical Methods in Biomedical Engineering **28**(6-7), 626–641 (2012). DOI 10.1002/cnm.1466. URL http://dx.doi.org/10.1002/cnm.1466

[30] Mynard, J.P., Smolich, J.J.: One-dimensional haemodynamic modeling and wave dynamics in the entire adult circulation. Annals of Biomedical Engineering pp. 1–18 (2015). DOI 10.1007/s10439-015-1313-8. URL http://dx.doi.org/10.1007/s10439-015-1313-8

[31] Olufsen, M.S., Peskin, C.S., Kim, W.Y., Pedersen, E.M., Nadim, A., Larsen, J.: Numerical simulation and experimental validation of blood flow in arteries with structured-tree outflow conditions. Annals of Biomedical Engineering **28**, 1281–1299 (2000)

[32] Pant, S., Fabrèges, B., Gerbeau, J.F., Vignon-Clementel, I.: A methodological paradigm for patient-specific multi-scale cfd simulations: from clinical measurements to parameter estimates for individual analysis. Int. J. Numer. Meth. Biomed. Eng. **30**(12), 1614–1648 (2014)

[33] Reymond, P., Bohraus, Y., Perren, F., Lazeyras, F., Stergiopulos, N.: Validation of a patient-specific one-dimensional model of the systemic arterial tree. American Journal of Physiology - Heart and Circulatory Physiology **301**(3), H1173–H1182 (2011). DOI 10.1152/ajpheart.00821.2010

[34] Reymond, P., Merenda, F., Perren, F., Rüfenacht, D., Stergiopulos, N.: Validation of a one-dimensional model of the systemic arterial tree. American Journal of Physiology - Heart and Circulatory Physiology **297**, H208–H222 (2009)

[35] Thomaseth, K., Cobelli, C.: Generalized sensitivity functions in physiological system identification. Ann. Biomed. Engnr. **27**, 607–616 (1999)

[36] Toro, E.F.: Riemann Solvers and Numerical Methods for Fluid Dynamics: A Practical Introduction, third edn. Springer-Verlag (2009). ISBN 978-3-540-25202-3

[37] Toro, E.F., Siviglia, A.: Flow in collapsible tubes with discontinuous mechanical properties: mathematical model and exact solutions. Communications in Computational Physics **13**(2), 361–385 (2013)

[38] Toro, E. F. and Millington, R. and Nejad, L. A. M.: Towards very high order Godunov schemes. In: E.F. Toro (ed.) Godunov Methods. Theory and Applications, vol. 1, pp. 897–902. Kluwer/Plenum Academic Publishers, New York, Boston and London (2001). Conference in Honour of S K Godunov

[39] Wan, S., Van Der Merwe, R.: The unscented Kalman filter for nonlinear estimation. In: Adaptive systems for signal processing, communications, and control symposium, pp. 153–158 (2000)